Title: Hyperinsulinemia acts via acinar insulin receptors to drive obesity-associated pancreatic cancer initiation by promoting digestive enzyme production and inflammation

Authors: Anni M.Y. Zhang[1], Yi Han Xia[1], Jeffrey S.H. Lin[1], Ken H. Chu[1], Wei Chuan K. Wang[1], Titine J.J. Ruiter[1], Jenny C.C. Yang[1], Nan Chen[1], Justin Chhuor[1], Shilpa Patil[1], Haoning Howard Cen[1], Elizabeth J. Rideout[1], Vincent R. Richard[3], David F. Schaeffer[2], Rene P. Zahedi[3,4,5], Christoph H. Borchers[3,6], James D. Johnson[1] *, Janel L. Kopp[1] *

Affiliations: [1]Department of Cellular and Physiological Sciences, Life Sciences Institute, University of British Columbia, Vancouver, Canada; [2]Department of Pathology and Laboratory Medicine, University of British Columbia, Vancouver, Canada; [3]Segal Cancer Proteomics Centre, Lady Davis Institute, Jewish General Hospital, McGill University, Montreal, Canada. [4]Department of Internal Medicine, University of Manitoba, Winnipeg, Canada. [5]Manitoba Centre for Proteomics and Systems Biology, Winnipeg, Canada. [6]Gerald Bronfman Department of Oncology, Jewish General Hospital, McGill University, Montreal, Canada.

***Correspondence**: janel.kopp@ubc.ca or james.d.johnson@ubc.ca

Keywords: pancreatic ductal adenocarcinoma, PanIN, hyperinsulinemia, obesity, insulin resistance

Funding: The project was supported by CIHR grants to E.J.R. (PJT153072), J.L.K. (MOP142216 and PJT162239) and J.D.J. (PJT168854) and by a Lustgarten Foundation Therapeutics Focused Research Program grant to J.D.J. and J.L.K. A.M.Y.Z. was supported by Frederick Banting and Charles Best Canada Graduate Scholarships and a Four-Year Fellowship from the University of British Columbia. J.L.K. was supported by a CIHR New Investigator Award (MSH147794) and the MSFHR Scholar Award (18309). E.J.R. was supported by the CIHR Sex and Gender Chair Program (GSA171465) and the MSFHR Scholar Award (16876). C.H.B. is grateful to Genome Canada for financial support through the Genomics Technology Platform (GTP264PRO) and the Quebec Cancer Consortium, Ministère de l'Économie et de l'Innovation, Quebec. C.H.B. is also grateful for support from the Segal McGill Chair in Molecular Oncology at McGill University (Montreal, Quebec, Canada), and for support from the Warren Y. Soper Charitable Trust and the Alvin Segal Family Foundation to the Jewish General Hospital (Montreal, Canada).

Author Contributions: A.M.Y.Z. designed, managed, and conducted the project including acquiring and interpreting the majority of the data and she wrote the manuscript. Y.X. performed proteomics and phospho-proteomics analyses. K.H.C. and J.C. provided technical assistance with pancreas sectioning and staining. J.S.H.L. and T.J.J.R. provided technical assistance with dissection and genotyping and J.S.H.L. performed the explant experiments. J.C.C.Y. provided technical assistance with dissection and staining. N.C. and W.C.K.W. analyzed staining. S.P. assisted with dissection and sample preparation and analyzed staining. H.H.C. assisted with proteomics and RNAseq analyses. E.J.R. evaluated the manuscript and helped with interpretation of the data in a sex-specific manner. V.R.R., R.P.Z., and C.H.B. co-designed and conducted proteomic analyses. D.F.S. provided histopathology analysis and expertise. C.H.B., J.L.K., and J.D.J. supervised the project, obtained funding, interpreted the data, and edited the manuscript. J.L.K. is the guarantor of this work.

Acknowledgements: The authors thank members from Johnson and Kopp labs for discussions. We thank Christopher Wright (Vanderbilt, USA) for the *Ptf1a*^{CreER} mice. RNA sequencing analysis was performed with the help of the SBME-Seq facility at UBC. Bioinformatics support was provided by Stephane Flibotte at the UBC Life Sciences Bioinformatics Core.

Conflict of interest: The authors report no relevant conflicts of interest.

Availability of data and materials: All data generated and analyzed in this study is included within the article, additional files, or is available from the corresponding author on request.

ABSTRACT

The rising incidence of pancreatic cancer is largely driven by the skyrocketing prevalence of obesity and type 2 diabetes (T2D). Hyperinsulinemia is a cardinal feature of both conditions, and is independently associated with increased cancer incidence and mortality. Our previous studies demonstrated that genetically reducing insulin production suppressed formation of pancreatic intraepithelial neoplasia (PanIN) pre-cancerous lesions in mice with mutant *Kras*. However, we found that hyperinsulinemia affected many cell types in the pancreatic microenvironment. Thus, it remained unclear whether hyperinsulinemia exerted its effects directly on the cells that give rise to PanINs or indirectly. The molecular mechanisms involved were unknown. Here, we tested whether insulin receptors (*Insr*) in *Kras*^{G12D}-expressing pancreatic acinar cells are necessary for the effects of hyperinsulinemia on obesity-associated pancreatic cancer development. Loss of *Insr* in Kras^{G12D}-expressing acinar cells did not prevent hyperinsulinemia or weight gain associated with high fat diet consumption in mice. However, solely reducing *Insr* in Kras^{G12D}-expressing acinar cells significantly reduced formation of PanIN and tumors, in a gene dose-dependent manner. Mechanistically, proteomic analyses showed that hyperinsulinemia acts through *Insr* to drive the excess production of digestive enzymes in acinar cells by modulating the activity of the spliceosome, ribosome, and secretory machinery. This increased local inflammation was abrogated by acinar-specific *Insr* knockout. We confirmed that insulin increased the conversion of wild-type acinar cells into acinar-to-ductal metaplasia in a trypsin- and *Insr*-dependent manner. Collectively, these data demonstrate that hyperinsulinemia acting via acinar cells insulin receptors promotes inflammatory conditions that cooperate with Kras signaling to increase the risk of developing pancreatic cancer, mechanistically linking obesity and pancreatic cancer.

INTRODUCTION

The 5-year survival rate of pancreatic ductal adenocarcinoma (PDAC) is less than 10% and it is projected to become the 2nd leading cause of cancer death by 2030[1]. Chronic pancreatitis, family history, smoking, obesity, and T2D are risk factors for pancreatic cancer[2]. Obesity and T2D are usually accompanied by hyperinsulinemia, hyperglycemia, increased inflammation, and dyslipidemia, which have all been proposed as underlying factors that drive the increased PDAC morbidity and mortality in this patient population[3,4]. Epidemiological studies consistently show that hyperinsulinemia is associated with increased risk of developing PDAC and worse survival[5,6]. Consistent with these epidemiological studies, experimentally inducing a hyperinsulinemic state in mice by feeding them a diet high in fat content consistently promotes tumor initiation in the pancreas when compared to chow fed mice[7,8]. Furthermore, we previously demonstrated that genetically limiting the high-fat diet mediated increases in insulin, reduced PDAC development, independently of hyperglycemia[9,10].

Single-cell analysis revealed that hyperinsulinemia altered gene expression in multiple cell types in the PanIN microenvironment[10], leaving open the question of whether the protective effects of reduced insulin production are direct on the tumor precursor cells or whether they are mediated indirectly by local immune cells, local fibroblasts, and/or via distant effects on adiposity[11-13]. Consistent with a direct effect on the epithelium, insulin stimulates proliferation in the PANC-1 and HPDE cell lines *in vitro*[14], but this does not provide information on the initiation of PDAC *in vivo*.

Altered insulin/IGF signaling, which includes cascades involving KRAS/MAPK/ERK and PI3K/AKT/mTOR, is prominent in human and animal pancreatic cancer. Activating mutations in *KRAS* are detected in >95% of PDAC clinical cases and induce PanIN pre-cancerous lesions and tumours in mice[15]. Activating mutations in *PIK3CA* are found in 3-5% of PDAC patients[16,17] and can initiate PDAC in mice[18], while silencing *Pik3ca* was protective in *Pdx1*-Cre;*Kras*$^{LSL-G12D}$;*Trp53*$^{LSL-R172H}$ mice[19]. Strategies that systemically reduce signaling downstream of Insr/Igf1r can suppress PDAC[18,20], but they do not distinguish between the roles for insulin, IGFs, or other upstream growth factors. Despite indirect evidence for an important role of insulin/IGF signaling in this and other cancers[3,4], a direct and causal role for the insulin receptor (*Insr*) alone has not been demonstrated for any cancer. Insr protein is increased in some breast, prostate, and liver cancers[21-23], but its role in the pancreas remains enigmatic.

In this study, we tested the hypothesis that hyperinsulinemia-induced enhancement of PDAC initiation is mediated through direct Insr signaling in pancreatic acinar cells. We found mice that consumed a high fat diet had a significant reduction in PanIN and tumor development when they lacked *Insr* specifically in Kras^{G12D}-expressing acinar cells. These findings indicate that hyperinsulinemia directly contributes to pancreatic cancer initiation through Insr in acinar cells via a mechanism that involves increased production of digestive enzymes and subsequent pancreatic inflammation.

RESULTS

Effects of acinar specific *Insr* loss on body weight and glucose homeostasis

To test our primary hypothesis, that hyperinsulinemia drives pancreatic cancer development via Insr cell autonomously, we generated mouse models in which *Kras*^{G12D} expression[24] and loss of *Insr* were both induced in acinar cells. Our cohorts contained mice with full *Insr* gene dosage, *Ptf1a*^{CreER};*Kras*$^{LSL-G12D}$;*Insr*$^{w/w}$;nTnG (PK-*Insr*$^{w/w}$); mice with partially reduced *Insr*, *Ptf1a*^{CreER};*Kras*$^{LSL-G12D}$;*Insr*$^{w/f}$;nTnG (PK-*Insr*$^{w/f}$); or knockout mice without any *Insr*, *Ptf1a*^{CreER};*Kras*$^{LSL-G12D}$;*Insr*$^{f/f}$;nTnG (PK-*Insr*$^{f/f}$) in Kras^{G12D}-expressing acinar cells (Figure 1A). We also generated a limited number of *Ptf1a*^{CreER};*Insr*$^{w/w}$;nTnG and *Ptf1a*^{CreER};*Insr*$^{f/f}$;nTnG mice to assess the baseline roles of *Insr* in acinar cells (Figure 1A). All mice were fed HFD (Figure 1B), which is known to produce sustained

hyperinsulinemia and accelerate PanIN/PDAC development[7,8]. Tamoxifen was injected at 4 weeks of age to simultaneously induce expression of mutant *Kras*^{G12D} and nuclear GFP[25], as well as deletion of floxed *Insr* alleles, specifically in acinar cells (Figure 1B). As expected, mice consuming HFD gained weight over time (Figure 1C-D) and at 43.5 weeks weighed more than the average 38- or 33-gram weight expected for chow-fed 44-week-old male or female C57Bl6J mice, respectively[26] (see also data at Jax.org). Acinar *Insr* loss did not significantly affect the weight gain of male or female mice in the context of mutant *Kras* (Figures 1C-D), but the presence of mutant *Kras* allele affected the weight gain of both males and females over time compared to *Kras* wildtype mice (Figure 1C-D). This is consistent with previous reports that ADM- and PanIN-mediated disruption of pancreatic function blunted weight gain in *Pdx1Cre;Kras*^{G12D} mice[27]. Fasting glucose was not different between genotypes (Figures 1E-F). HFD induced similar levels of hyperinsulinemia in both genotypes (Figures 1G-H). As expected[9,10], males had higher insulin levels compared to females (Figures 1G-H). These insulin levels were well above chow diet-fed male C57Bl6J mice (138 +/- 24 pM)[28]. Our data demonstrate that acinar-specific *Insr* deletion does not have major effects on glucose homeostasis in mice. Thus, our model enabled us to test the role of acinar cell *Insr* in the context of hyperinsulinemia and normoglycemia, modelling the typical obese, non-diabetic state.

Acinar *Insr* knockout limits loss of normal pancreatic parenchyma by Kras^{G12D}

To test whether *Insr* loss affected Kras^{G12D}-mediated PDAC formation from acinar cells, we examined a cohort of 5-16 PK-*Insr*$^{w/w}$, PK-*Insr*$^{w/f}$, and PK-*Insr*$^{f/f}$ mice of each sex and genotype. We planned to quantify the extent of lesions at ~1 year of age based on the timing of our previous genetic models with reduced insulin[9,10], but half the male PK-*Insr*$^{w/w}$ mice and a few female PK-*Insr*$^{w/w}$ mice reached humane endpoint earlier (Figure 2A). Therefore, we chose to end the study at 43.5 weeks of age for Kras^{G12D} mice. Through necropsy and histology, we noted that PDAC was present in 4 male PK-*Insr*$^{w/w}$ mice, but more importantly, almost the entire parenchyma of male PK-*Insr*$^{w/w}$ mice was replaced by ductal metaplasia comprised of cysts, PanIN, and ADM (Figure 2A-C, E). Three male PK-*Insr*$^{w/f}$ mice reached humane endpoint prior to 43.5 weeks without macroscopic tumors (Figure 2A-B), but more animals of this genotype retained normal acinar cell area (Figure 2C, E). No male PK-*Insr*$^{f/f}$ mice reached humane endpoint by 43.5 weeks of age (Figure 2A-B) and they retained even more normal acinar cell area on average (Figure 2C, E). One female PK-*Insr*$^{w/w}$ mouse, as well as a 1 female PK-*Insr*$^{w/f}$ mouse, reached humane endpoint prior to 43.5 weeks of age, while no female PK-*Insr*$^{f/f}$ mice reached humane endpoint by 43.5 weeks of age (Figure 2A-B). No macroscopic tumors were noted at necropsy (Figure 2A-B), but histologically, we found that the incidence of PDAC in females was *Insr* dosage-dependent (Figures 2B, and D). The majority of female mice from every genotype retained some normal parenchyma (Figures 2D-E), potentially explaining why females reached humane endpoint less often than males. This is consistent with previous reports suggesting

that the timing and/or extent of lesion formation differs between male and female mice in the context of HFD[8]. Together, these data strongly suggested that limiting or eliminating insulin/Insr activity specifically in acinar cells reduced the propensity of HFD and Kras activation to transform the pancreas.

Loss of *Insr* in acinar cells reduces the extent of *Kras*^{G12D}-mediated lesion formation

We next quantified the extent of the tissue disruption and lesion formation only in mice that were 43.5 weeks of age to assess the extent of disease in the presence or absence of *Insr*. In parallel with PanIN quantification, we stained all pancreata for nuclear GFP from the nTnG lineage reporter allele[25]. As expected, most acinar cells and PanIN lesions were GFP positive (Figures S1A-B), confirming that the lesions arose from Ptf1a^{+} acinar cells. Pancreata from *Kras* wild-type *Ptf1a*^{CreER};*Insr*$^{w/w}$;nTnG and *Ptf1a*^{CreER};*Insr*$^{f/f}$;nTnG mice were similarly comprised of acinar cells and endocrine islets, and had broad GFP expression in acinar cells (Figures S1C-F). In contrast, pancreata from male and female PK-*Insr*$^{w/w}$, PK-*Insr*$^{w/f}$, and PK-*Insr*$^{f/f}$ mice all contained ductal lesions with histological characteristics of metaplastic ducts, including ADM, low-grade and high-grade PanIN, and sometimes PDAC tumors (see above; Figures 2C-D). Reducing *Insr* in Kras^{G12D}-expressing acinar cells decreased the area of PanINs plus tumors, PanIN alone, or tumor area in a dose dependent manner in males and females (Figures 2F-H). Consistent with this histological-based quantification, measuring the pancreatic area containing ductal metaplasia (ducts, ADM, PanIN and PDAC) or mucinous lesions (PanIN and some tumors) with Ck19 or Alcian blue staining, respectively, similarly showed that female PK-*Insr*$^{w/w}$ mice formed significantly more lesions than female PK-*Insr*$^{f/f}$ mice (Figures S2A-F). Notably, male PK-*Insr*$^{w/w}$ mice had a significantly higher amount of Ck19^{+} area, but a similar amount of Alcian blue^{+} area, compared to other genotypes (Figure S2A-F). This latter observation is likely explained by the presence of Alcian blue negative high-grade PanIN lesions and large cysts with predominantly normal ductal epithelium, which were more prevalent in male than female PK-*Insr*$^{w/w}$ pancreata (Figures 2C-D, S2A-F). Indeed, most male PK-*Insr*$^{w/w}$ and some female PK-*Insr*$^{w/w}$ pancreata were comprised of almost all Ck19^{+} area with little acinar cell area left, while larger areas of normal acinar cells correlated with lower Ck19^{+} areas in PK-*Insr*$^{w/f}$ and PK-*Insr*$^{f/f}$ mice (Figures 2C-E, S2G-H). Therefore, our data strongly suggested that acinar cell *Insr* dose-dependently regulates oncogenic Kras-induced PanIN formation in the context of diet-induced hyperinsulinemia.

Loss of *Insr* in *Kras*^{G12D}-expressing acinar cells blocks early PanIN initiation

To examine whether early PanIN initiation was specifically affected by loss of *Insr* in acinar cells, we examined mice at 12 weeks of age. At 8 weeks post-tamoxifen injection, acinar cells and PanIN lesions were also GFP positive indicating good recombination efficiency (Figure S3A-B). There were no significant differences in pancreas weight or Cpa1^{+} area between PK-*Insr*$^{w/w}$, PK-*Insr*$^{w/f}$, and PK-

Insr$^{f/f}$ mice in either sex, nor were there any differences in pancreatic weight of Kras^{G12D}-expressing mice compared to *Ptf1a*^{CreER};*Insr*$^{w/w}$;nTnG or *Ptf1a*^{CreER};*Insr*$^{f/f}$;nTnG mice (Figure S3C-G). This is consistent with previous data showing that the young pancreata from *Ptf1a*^{CreER};*Kras*$^{LSL-G12D}$ mice have relatively fewer PanIN lesions[24]. Pancreata from PK-*Insr*$^{f/f}$ mice were predominantly normal and had significantly fewer ductal lesions with ADM or low-grade PanIN characteristics when compared to PK-*Insr*$^{w/w}$ mice (Figure 3A-C). Consistent with the increased number of lesions in PK-*Insr*$^{w/w}$ compared to PK-*Insr*$^{f/f}$ mice, there was slightly less Cpa1^{+} area in female PK-*Insr*$^{w/w}$ compared to PK-*Insr*$^{f/f}$ pancreata (Figure S3C-E) and a weak inverse correlation of overall PanIN area to Cpa1^{+} area only for PK-*Insr*$^{w/w}$ mice (Figure S3F). Bulk RNA sequencing and gene ontology analyses also showed that PK-*Insr*$^{w/w}$ compared to PK-*Insr*$^{f/f}$ pancreata had higher expression of genes associated with Ras signaling, proliferation, and inflammation, which are typically associated with PanIN initiation[29] (Figure 3E-F, Table S1). The significant inhibition of PanIN formation at 12 weeks of age solely through reducing *Insr* in acinar cells strongly supported a model in which diet-induced hyperinsulinemia promoted tumor initiation through insulin receptor action on acinar cells.

Akt and Erk signaling are reduced in PanINs in the absence of *Insr*

Insulin receptor tyrosine kinases act through the PI3K/Akt/mTor and Mapk/Erk signaling cascades. To further assess the molecular changes associated with the loss of *Insr* in acinar cells, we examined the phosphorylation of Akt at S473 and the phosphorylation of Erk at Thr202/Tyr204 by immunohistochemistry (Figure S4). As previously shown[29], strong staining for pAkt and pErk was present in PanIN lesions in PK-*Insr*$^{w/w}$ pancreata (Figure S4A-F). As expected in the context of reduced insulin signaling, weaker signals for both phospho-specific Akt or Erk antibodies were found in the PanINs in PK-*Insr*$^{f/f}$ compared to PK-*Insr*$^{w/w}$ pancreata (Figure S4A-D). Although the pAkt and pErk signal decreased or changed localization in PanIN lesions in PK-*Insr*$^{f/f}$ mice, the pAkt^{+} signal was present in the stromal cells surrounding the PanIN lesions regardless of genotype (Figure S4A-D). These data suggest that loss of *Insr* in acinar cells can reduce PI3K/Akt/mTor and Mapk/Erk signaling during oncogenic Kras^{G12D}-mediated PanIN formation.

Pancreata from mice lacking acinar cell Insr have reduced digestive enzymes

To define the underlying molecular mechanisms of *Insr* action during PanIN initiation, we conducted unbiased total proteomic and phospho-proteomic analyses using the head of the pancreas from the 12-week-old female mice (Figure 3, Tables S2-S3) with and without Kras^{G12D} and/or *Insr*. For the total proteome dataset, we obtained reliable, quantitative data on 2889 proteins across all the samples. First, we examined the effects of mutant Kras in the context of normal *Insr*. Consistent with our histological analyses identifying a change in PanIN frequency, we found that the inflammation- and PanIN-associated proteins, Reg3a, Reg3b, Reg2, Tff1, Gkn1, Gkn2, and Agr2[30-33], were among the

124 proteins significantly enriched in PK-*Insr*$^{w/w}$ compared to *Ptf1a*^{CreER};*Insr*$^{w/w}$;nTnG pancreata (Figure 4A, Table S2). We also found that proteins associated with acinar cell function, such as Ctrc, Dbi, Pla2g1b, and Clps, were among the 122 proteins significantly down-regulated as a consequence of *Kras*^{G12D} expression in acinar cells (Figure 4A, Table S2). Other proteins associated with acinar cell function, like Cpa1, Spink1, and Cela1, remained unchanged between the PK-*Insr*$^{w/w}$ and *Ptf1a*^{CreER};*Insr*$^{w/w}$;nTnG genotypes (Table S2). We also compared the differentially expressed pathways between PK-*Insr*$^{w/w}$ and *Ptf1a*^{CreER};*Insr*$^{w/w}$;nTnG mice to differentially expressed pathways between human PDAC and normal pancreas tissues adjacent to human PDAC[34] and found concordance (Figure S5A-B), reinforcing the translational relevance of this model. Interestingly, we also found 92 proteins increased in abundance and 155 proteins had decreased abundance solely due to loss of *Insr* in Kras wild-type acinar cells (Figure 4B), with the caveat that we analyzed a low sample number. However, reductions in Ctrc, Clps, Pla2g1b in this analysis (Figure 4B, Table S2) suggested that *Insr* may have a role in regulating the function of wild-type acinar cells in mice fed HFD.

To define the molecular mechanisms associated with *Insr* deletion in the context of mutant Kras, we focused further analyses on comparing the PK-*Insr*$^{f/f}$ pancreata to the PK-*Insr*$^{w/w}$ pancreata. We found that 135 proteins were enriched and 117 were depleted in PK-*Insr*$^{f/f}$ mice compared to PK-*Insr*$^{w/w}$ controls (Figure 4C). We then performed a K-means clustering analysis with the abundance values of these differentially enriched proteins in all genotypes to identify groups of proteins that varied by *Insr* status, Kras mutation, or both (Figure 4D and Table S4-all clusters). In order to investigate potential functional enrichment of protein groups based on cell signaling, intracellular localization, and biological process, we also used the differentially abundant proteins between PK-*Insr*$^{w/w}$ and PK-*Insr*$^{f/f}$ mice to build protein-protein interaction networks using STRING[35] and assigned these proteins to their intracellular organelle locations in a diagram using the COMPARTMENTS section of GeneCards and/or existing knowledge of their function[36] (Figure 5A). As expected from our histological analyses, the total proteomics analyses confirmed that proteins associated with PanIN initiation or formation, such as Reg3a, Reg3b, Reg2, Tff1, Gkn1, and Gkn2, were higher in PK-*Insr*$^{w/w}$ pancreata compared to *Ptf1a*^{CreER}*;Insr*$^{w/w}$;nTnG and PK-*Insr*$^{f/f}$ pancreata (Figure 4C, 4D-cluster 1, 5A). Proteomic analyses highlighted the striking downregulation of the majority of the proteins packaged into zymogen granules for secretion in PK-*Insr*$^{f/f}$ compared to *Ptf1a*^{CreER};*Insr*$^{w/w}$;nTnG and PK-*Insr*$^{w/w}$ mice (Figure 4D-cluster 2,3, 5A-B). Acinar cells produce a large amount of protein every day and in *Ptf1a*^{CreER};*Insr*$^{w/w}$;nTnG mice and PK-*Insr*$^{w/w}$ pancreata fed HFD ~19% of all the peptides detected in our analyses were associated with the zymogen granules (Figure 5C). However, this percentage was reduced significantly to 12.2% in PK-*Insr*$^{f/f}$ pancreata (Figure 5C). This reduction in zymogen granule proteins is likely an underestimation of the effect on the total proteome, as our differential abundance analyses

were normalized to total protein content. In sum, loss of *Insr* in acinar cells resulted in a coordinated decrease in digestive enzymes produced by acinar cells in the context of HFD.

Insr signaling regulates the post-transcriptional synthesis of digestive enzymes

Pancreatic acinar cells represent the cellular majority in our bulk tissue proteome. With the caveat that our bulk tissue includes multiple cell types, our STRING network analysis nevertheless highlighted mechanisms downstream of *Insr* loss that underlie this dramatic reduction in zymogen granule content in acinar cells. This included increases in proteins with key roles in suppressing protein synthesis at the ribosome (eEF2K), as well as increases in the first enzyme of the fatty acid beta oxidation pathway (Acox1), a protein regulating lysosome function (Grn), and protein processing machinery at the ER and Golgi (Ilvbl, Ssr3, Ssr4, Irag2). Many components of mitochondrial electron transport complexes were changed, as well as endosomal and cytoskeletal proteins, many of which are involved in moving organelles within the cells or in exocytosis, such as Snx5, Vps35l, Sycn (Figure 5A). Finally, we also found decreases in critical parts of the spliceosome (Snrpa), the signal recognition particle complex receptor (Srprb), and components of the large ribosome (Rpl29, Rpl36, Rpl37a). These observations suggested that loss of *Insr* in acinar cells and a reduction in PanIN formation was associated with a post-transcriptional reduction in the synthesis of digestive enzymes.

***Insr* loss in acinar cells reduced phosphorylation of proteins involved in translation**

Parallel phosphoproteomic analysis identified 225 downregulated phospho-peptides and 177 upregulated phospho-peptides by comparing the PK-*Insr*$^{f/f}$ pancreas to PK-*Insr*$^{w/w}$ controls (Figure 6A-D, Table S3). In general, statistically significant phospho-peptide differences were not due to underlying differences in total protein abundance (Figure 6B, Table S5). As above, we mapped the location and function of the modified proteins (Figure 6C-D). Specifically, we found significant decreases in phosphorylation in PK-*Insr*$^{f/f}$ compared PK-*Insr*$^{w/w}$ pancreata for proteins involved in transcription elongation (Eloa, Top2a, Supt5h), mRNA splicing and nuclear speckle formation (Srpk1, many Srsf proteins, Cherp, Srrm1 and Srrm2), as well as protein translation initiation (Eif4b, Eif5b, and eIF3 complex proteins) and elongation (Eef1b, Eef1d, and many ribosomal subunits). There were also decreases in phospho-peptides for Cavin3, which has been implicated in Akt-Erk signaling bias[37,38], and the PP1 inhibitor Ppp1r2, at sites known to be influenced by insulin signaling (Figure 6D). There was also reduced phosphorylation of Larp1 at sites known to be regulated by mTorc1 component, Raptor[39]. Larp1 is an RNA-binding protein that links mTorc1 to the translational regulation of terminal oligopyrimidine tract containing mRNAs that encode for ribosomal proteins and elongation factors[40]. Together, our proteomics data suggested that Insulin/Insr promotes the production of proteins in acinar cells in part through its modulation of Larp1 and many other components controlling transcription, translation, and secretion of digestive enzymes. Interestingly, multiple sites on the

cholecystokinin (Cck) receptor (Cckar) also showed altered phosphorylation (Figure 6C-D), including sites in the main intracellular loop that are indicative of ligand-induced desensitization[41] and phospho-sites in the C-terminal tail that have not been previously reported. Collectively, these unbiased and quantitative (phospho)proteomic analyses delineate molecular mechanisms by which hyperinsulinemia, acting via the Insr, may promote Kras-driven pancreatic cancer initiation.

Reducing insulin receptor signaling in acinar cells reduces fibrosis and inflammation

Our histological analyses, as well as our total proteomics and phosphoproteomics suggested that loss of the *Insr* in acinar cells prevented the formation of PanIN and prevented the induction of genes associated with pancreatic injury, such as Reg3a, Reg3b, and Reg2. To examine whether loss of *Insr* in acinar cells reduced the injury, inflammation, and/or fibrosis typically associated with $Kras^{G12D}$ activation and PanIN formation, we imaged Sirius Red, alpha smooth muscle actin (αSMA), and F4/80 in 12-week-old pancreata (Figures 7A-B, S6A-D) to quantify the amount of collagen, activated fibroblasts, and macrophages present in the stroma. In PK-$Insr^{w/w}$ control pancreata, Sirius Red, αSMA, and F4/80 staining surrounded the metaplastic ducts, containing ADM and PanIN, as well as the surrounding acini in nearby lobules (Figures 7A-B, S6A-D). In contrast, in the PK-$Insr^{f/f}$ pancreata, the metaplasia that did form tended to be associated with less Sirius Red, αSMA, and F4/80 staining, as well as lower levels of staining in the neighboring lobules (Figures 7A-C, S6A-F). This supported our hypothesis that inflammation was reduced in the absence of *Insr* in $Kras^{G12D}$-expressing acinar cells.

Trypsin inhibitors block the effects of insulin on acinar-to-ductal metaplasia

Our proteomics data suggested reduced abundance of digestive enzymes in the absence of *Insr* in acinar cells in the context of $Kras^{G12D}$ (Figure 5). Given that autoactivation of trypsinogen in acinar cells or in the pancreatic parenchyma may contribute to the induction of pancreatitis[42], we reasoned that the reduced presence of enzymes in the absence of *Insr* could lessen tissue damage that spreads to other lobules. This would result in decreased ADM and PanIN formation, as in the PK-$Insr^{f/f}$ pancreata. To test this hypothesis, we utilized an 3D *ex vivo* model of ADM formation from acinar cells (Figure 7D)[43,44] to determine whether insulin levels affected the acinar to ductal transition. Acinar cells were isolated from wild-type male or female CD1 or Bl6 mice fed a normal chow diet. Wild-type female and male acinar cell clusters grown in collagen for 5 days predominantly maintained their acinus morphology, as previously shown (Figure 7E-CD1; male CD1 and Bl6 data not shown)[43]. TGF-α induced these clusters to form a duct-like lumen structure (Figure 7E-F-Cd1 female, Figure S7A-Bl6 female)[45]. Male acini typically did not form ring structures in response to TGF-α (Figure S7A-Bl6; CD1-data not shown), therefore we used female acini to test our hypothesis. Increasing concentrations of

insulin significantly potentiated TGF-α induced ring formation (Figure 7E-F). Remarkably, the synergism between insulin and TGF-α was completely blocked by trypsin inhibitor (Figure 7F). Acini from *Ptf1a*^{CreER};*Insr*$^{f/f}$;nTnG mice formed fewer ADM rings with or without TGF-α, and were unaffected by insulin (Figure 7G), demonstrating that these effects of insulin were mediated via *Insr*. Together, our data demonstrated that hyperinsulinemia-mediated trypsinogen pro-enzyme overproduction of, and subsequent autoactivation[46], promotes local inflammation and initiation of PanIN lesions (Figure 7H).

DISCUSSION

The purpose of this study was to test the hypothesis that hyperinsulinemia in the obese state acts directly on acinar cells to promote pancreatic cancer initiation. Our data clearly support a model where Insr in acinar cells plays a causal role in supporting cancer initiation in the context of diet-induced obesity and mutant Kras. The contribution of direct insulin action on acinar cells during initiation from normal cells explains a large portion of the effects of obesity, but our results do not formally preclude minor roles for Insr in other local or distant cell types[10]. Our unbiased proteomic and phospho-proteomic analyses led us to propose a model in which diet-induced hyperinsulinemia acts directly on Insr in acinar cells to promote the physiological function of acinar cells, which is to supply digestive enzymes to break down lipid rich food in the duodenum. However, the increased production of enzymes increases the risk that more autoactivated trypsin will be present, as well. This increased propensity for trypsin-induced injury would result in sub-clinical levels of inflammation and acinar-to-ductal metaplasia. In the context of *Kras* mutations, this increased production can lead to increased chances of inflammation, which are known to enhance Kras^{G12D} signaling and promote an irreversible transformation in Kras^{G12D}-expressing acinar cells[47]. Thus, our studies provide a key missing link explaining the connection between obesity and hyperinsulinemia and increased pancreatic inflammation and PanIN initiation.

Diet-induced obesity induces insulin hypersecretion, increases beta cell mass, and impairs insulin clearance resulting in sustained hyperinsulinemia[4,11]. Mice used in this study, which had the full complement of all 4 insulin alleles (*Ins1* and *Ins2*), exhibited higher fasting insulin levels (males 1000-1500 pmol/L; females 500 pmol/L) than our previous models with insulin gene dosage reduced to 1 or 2 copies (males, 400-800 pmol/L; females 100-200 pmol/L)[9,10]. The gradation of insulin levels between mice replete with insulin and those with reduced insulin production, is reflected in the severity of normal pancreas replacement by ductal metaplasia, PanIN, and tumors (e.g. this study PK-*Ins1*$^{+/+}$:*Ins2*$^{+/+}$ ~90% replaced, PK-*Ins1*$^{+/+}$;*Ins2*$^{-/-}$ ~25% replaced, PK-*Ins1*$^{-/-}$;*Ins2*$^{+/+}$ ~1-4% replaced[9,10]). These findings reinforce that simply reducing insulin production limits PanIN initiation in the context of obesity.

All cells in the body have insulin receptors and require insulin signaling for key functions, including nutrient uptake for storage and anabolism. While the roles of Insr in hepatocytes, myocytes, and adipocytes are well studied[48-50], the consequences of *Insr* loss in pancreatic acinar cells remain understudied. In this study, we specifically deleted the *Insr* gene from acinar cells using the *Ptf1a*^{CreER} allele and showed that insulin insensitivity in acinar cells had no obvious effects on systemic glucose homeostasis or serum insulin levels regardless of the *Kras* gene status. This suggests that the systemic regulation of glucose and insulin homeostasis are similarly perturbed in our mice fed HFD. Our data, combined with our previous studies[9,10], effectively rule out an essential role for hyperglycemia in PanIN and PDAC formation, but do not preclude roles for hyperglycemia in the later stages of disease[51,52].

Insr signaling activates mitogenic PI3K/AKT/mTOR and MAPK/ERK signaling cascades that are frequently mutated during tumorigenesis[53-55], including in pancreatic cancer. Indeed, activating mutations in Kras, a key mediator of insulin and insulin-like growth factor signaling, drive the vast majority of pancreatic cancers[15]. Previous *in vitro* evidence supported the concept that hyperinsulinemia could promote cancer cell growth through over-activating the signaling cascades downstream of Insr protein[3,4,56,57]. Our findings show that insulin has a direct causal role in promoting the metaplastic changes needed for the acinar cell of origin to initiate tumorigenesis.

Mechanistically, our proteomic data demonstrate that *Insr* loss in acinar cells results in the coordinated reduction in digestive enzymes, with or without mutant Kras. Our observations confirm that insulin signaling normally supports exocrine function and are consistent with previous studies showing that amylase production is diminished by β-cell ablation using streptozotocin and restored with insulin injection[58-60]. The tendency towards reduced body weight in mice lacking acinar-cell Insr at some ages is also consistent with sub-clinical pancreatic insufficiency and a relative reduction in the ability to utilize ingested nutrients. Mutations that result in increased trypsin activity in the pancreas[8], as well as animal studies using the Cck analog, caerulein, to stimulate enzyme secretion at supraphysiological levels[61], support the concept that tight control of digestive enzyme function reduces the risk of PDAC. Our phospho-proteomic data identified hyper-phosphorylation of the Ccka receptor in *Insr*-knockout pancreas, linking local insulin signaling to Cck, a key endogenous regulator of acinar cell function and pancreatic weight[62-64]. It has been reported that HFD-associated inflammation can also promote islet Cck expression, which was proposed to play a role in obesity-associated PanIN formation[65]. Ultimately, our data indicate that hyperinsulinemia, acting through Insr, is the upstream driver of diet-induced inflammation via hyperactive digestive enzyme production (Figure 7H). *Insr* loss in acinar cells counters the increased signal for acinar cell enzyme production or cell proliferation induced by HFD. Further studies are needed to fully understand the impact of dietary content on acinar cells and their susceptibility to Kras^{G12D}-mediated transformation.

Our proteomic analyses revealed other key mechanisms associated with suppressed pancreatic cancer initiation from acinar cells lacking *Insr*. For example, mRNA splicing and translation factors, known targets of insulin signaling via mTor[49], are differentially abundant in the pancreas after *Insr* loss in $Kras^{G12D}$-expressing acinar cells, suggesting mechanisms by which insulin may regulate digestive enzyme production. We also found evidence that reduced insulin signaling affects cellular metabolism. Previous studies suggested that insulin promotes glycolysis in wildtype acinar cells to protect them during pancreatitis[66], however, detailed analyses of cell-type-specific mechanisms await single-cell proteomic and single-cell metabolomic characterization of this model.

In summary, our data strongly suggest that insulin receptor signaling in acinar cells contributes to the PanIN and PDAC development. Our data illustrate the complex and interconnected molecular mechanisms by which hyperinsulinemia, acting directly through acinar cell Insr, promotes early pancreatic tumourigenesis. Thus, we can infer that targeting insulin receptor signaling pathways, or hyperinsulinemia itself, may be beneficial in treating and preventing pancreatic cancer. The ligand of this pathways, insulin, is one of the most clinically actionable hormones in our bodies and it can be easily measured and can be modulated by diet, exercise, as well as FDA-approved drugs. Thus, our novel observations that modifying insulin alone can reduce the risk of initiating PDAC elucidate multiple prevention strategies that could be trialed in humans.

Limitations of the Study

While our study breaks new ground, we also acknowledge its limitations and scope. Our results led to a focus on cancer initiation, so we cannot extrapolate these findings and models to our understanding of advanced tumor progression or metastasis. Futures studies will be needed to dissect the role of hyperinsulinemia and insulin receptors on these later stages.

Some of our data, including non-significant trends, are suggestive of sex differences in the role of Insr mechanisms and/or interactions between PDAC initiation and whole-body glucose homeostasis. Additional work, beyond the scope of this study, will be required to investigate this. We think it is unlikely that the mechanistic role of Insr is fundamentally different between sexes, although it seems possible that inherent differences in male and female acini affect their predisposition to undergo metaplasia in the mouse.

A technical limitation of our study, and the field, is that existing antibody reagents are not specific enough to perform accurate anti-Insr staining that would allow us to determine whether acinar cells that contributed to PanIN formation did so due to incomplete recombination at the *Insr* floxed allele. Moreover, coverage of the proteome was not complete and biased against membrane proteins. For example, analysis of the abundance and phosphorylation of Igf1r, a protein that may compensate in *Insr* knockout cells, will require targeted assays and/or membrane fractionation. Insulin could bind to homodimeric Igf1 receptors and heterodimeric Insr/Igf1r hybrids, although at a lower affinity[21], to

mediate its pro-tumourigenic effects. Future studies on acinar cell-specific *Igf1r* knockout and/or *Insr*/*Igf1r* double knockout would be necessary to delineate any *Igf1r* contribution to PanIN formation. Nevertheless, it is clear that simply reducing *Insr* gene dosage was sufficient to reduce the effects of hyperinsulinemia on PanIN initiation.

METHODS

RESOURCE AVAILABILITY

Lead contact

Further information and requests for resources and reagents should be directed to and will be fulfilled by the lead contact, Janel Kopp (janel.kopp@ubc.ca).

Materials availability

Mouse lines and cell lines generated in this study are available from the lead contact upon request.

Data and code availability

- Proteomics, phosphoproteomics and RNA-seq data have been deposited in the Gene Expression Omnibus and ProteomeXchange Consortium via the PRIDE and are publicly available as of the date of publication. Accession numbers are listed in the key resources table. Microscopy data reported in this paper will be shared by the lead contact upon request. Source data for the figures in the manuscript are available as Data S1: Sources.
- All original code has been deposited at https://github.com/johnsonlabubc/PDAC-Insr-KO-Total-and-Phosphoproteomic-Analysis and is publicly available as of the date of publication. DOIs are listed in the key resources table.
- Any additional information required to reanalyze the data reported in this paper is available from the lead contact upon request.

EXPERIMENTAL MODEL AND SUBJECT DETAILS

Mouse models

All animal experiments were conducted at the University of British Columbia with approval of the University of British Columbia Animal Care Committee in accordance with Canadian Council for Animal Care guidelines. All alleles have been described previously[24,67-71]. *Kras*$^{LSL\text{-}G12D/w}$ (#008179), *Insr*$^{f/f}$ (#006955), and nuclear TdTomato-to-nuclear EGFP (nTnG) mice (#023035) were purchased from Jackson Labs (Bar Harbour, USA). *Ptf1a*$^{CreER/w}$ mice (C57BL/6) were a gift from Chris Wright (Vanderbilt, USA). Mice were maintained on C57BL/6 genetic background and housed at the University of British Columbia Modified Barrier Facility which was temperature-controlled (22°C) and specific pathogen-free. They were kept on a 12:12 hr light: dark cycle with food and drinking water *ad libitum*. To generate genetic background-matched *Ptf1a*$^{CreER/w}$*;Kras*$^{LSL\text{-}G12D/w}$*;Insr*$^{w/w}$*;nTnG*, *Ptf1a*$^{CreER/w}$*;Kras*$^{LSL\text{-}G12D/w}$*;Insr*$^{w/f}$*;nTnG*, and *Ptf1a*$^{CreER/w}$*;Kras*$^{LSL\text{-}G12D/w}$*;Insr*$^{f/f}$*;nTnG* mice, *Ptf1a*$^{CreER/w}$*;Kras*$^{LSL\text{-}G12D/w}$*;Insr*$^{w/f}$*;nTnG* mice were bred with *Insr*$^{w/f}$ mice. After weaning (3 weeks), the

resulting litters were fed with high fat diet (HFD), and at 4 weeks of age, recombination was induced over three consecutive days by subcutaneous injections of tamoxifen in corn oil (20 mg/mL) of 5 mg tamoxifen/40 g body mass. Both male and female mice were used in this study and humane endpoint was met in this study by losing 20% of the max body weight. One cohort of mice was euthanized at 10 months of age for histopathology analyses and the whole pancreas was used for histopathology analyses. Another cohort of mice was euthanized at 12 weeks of age. For mice euthanized at 12 weeks, each pancreas was cut into three pieces roughly based on the pancreas anatomical structure: head, body, and tail. The body piece was used for histopathological analyses, while the other pieces were snap frozen in liquid nitrogen and kept at -80 °C. The head piece was processed for proteomics and phospho-proteomics analyses and part of the tail was used for RNA analyses (see below).

METHOD DETAILS

Assessment of glucose homeostasis

Mouse body weight and fasting blood glucose levels were measured every 4 weeks and fasting insulin were measured every 3 months. Before the measurements, mice were fasted for 4 hours in clean and fresh cages during the light period. One drop of blood was collected from each mouse's saphenous vein and a Lifescan OneTouch Ultra Mini glucometer was used to measure the fasting blood glucose levels. About 30 µl of blood was collected with a heparinized microhematocrit capillary tube (Fisher Scientific, 22-362566, Waltham, MA, USA) for measuring fasting insulin levels. The collected blood was centrifuged at 10,000 rpm for 10 minutes to collect the blood serum. Then the blood serum was kept at -20°C until used to measure the fasting insulin levels with insulin ELISA (80-INSMSU-E10; ALPCO Diagnostics, Salem, NH).

Histopathological, morphological, and immunohistochemical analyses

Pancreata were fixed in 4% paraformaldehyde for 24 hours at 4°C followed by paraffin embedding. Mouse pancreata were sectioned then stained with hematoxylin and eosin (H&E), anti-GFP immunohistochemistry, or Alcian blue, as described[9,10,72]. The stained slides were scanned with a 20x objective using a 3DHISTECH Panoramic MIDI (Quorum Technologies Inc. Guelph, Canada) slide scanner. One 12-week-old mouse with a GFP labeling efficiency of acinar cells below 20% was excluded from further analyses. Histopathological analyses were conducted in a de-identified manner and verified separately by J.L.K and D.F.S. All histopathological analyses were performed on one of the stained sections that displayed the maximal pancreatic cross-sectional area unless otherwise stated. Every gland with a lumen was categorized as normal, ADM, PanIN, or neoplasia, and glands representing more than one of these categories were scored based on their highest-grade feature. The total pancreatic area, PanIN plus tumor area, PanIN area, or normal acinar cell area were

measured as previously described[9,10]. Briefly, the total pancreatic area, PanIN plus tumor area, PanIN area, or normal acinar cell area was determined by masking all pancreatic tissue, selective masking of the PanIN plus tumor area, selective masking of the only PanIN area, or selective masking of the normal acinar cell area by Adobe Photoshop. Pixels for the total pancreatic area or each histological feature were measured by ImageJ and this was used to calculate the percentage area occupied by each histological feature. For Alcian blue positive area, Adobe Photoshop 2020 Black & White function was used to highlight the blue area (red filter). The total pixels for pancreas or Alcian blue positive area were counted using ImageJ. For Sirius Red positive area, Adobe Photoshop 2020 Black & White function was used to highlight the red area (green filter). The total pixels for pancreas or Sirius Red positive area were counted using ImageJ. Immunohistochemistry and immunofluorescence staining was performed according to published standard protocols[10,24,72]. Primary antibodies were rabbit anti-cytokeratin 19 (Ck19) (Abcam, ab133496, 1:1000), mouse αSMA (Sigma Aldrich, A2547, 1:100) and goat anti-GFP (Abcam, ab6673, 1:200). Secondary antibodies were Cy3 conjugated AffiniPure Donkey Anti-Rabbit IgG (Jackson ImmunoResearch, 711-165-152, 1:500), biotin-conjugated donkey anti-rabbit (Jackson ImmunoResearch, 711-065-152, 1:500), or biotin-conjugated rat anti-goat (Vector Laboratories, MP-7404, 1:2). Slides were scanned with a 20x objective using a 3DHISTECH Panoramic MIDI slide scanner. Ck19, Cpa1, pErk, pAkt, or F4/80 positive areas or αSMA positive area was measured with Adobe Photoshop 2020 using the Black & White function to filter and highlight the brown area (blue filter) or the red fluorescence area, respectively, which was then taken as a percent of pixels in the pancreatic section.

RNA isolation and analysis

A piece of the tail from pancreata collected from female mice at 12 weeks of age (PK-*Insr*$^{w/w}$ (n=4), PK-*Insr*$^{w/f}$ (n=3), PK-*Insr*$^{f/f}$ (n=4)), were frozen with liquid nitrogen and shattered with a C01 Manual Pulverizer and RNA was isolated with RNeasy Micro Kit (QIAGEN, 74004). After RNA extraction, the Agilent 2100 Bioanalyzer was used to perform sample quality control. Samples that qualified (RIN>5) were prepped using the standard protocol for Illumina Stranded mRNA prep (Illumina). Sequencing was done using the Illumina NextSeq 2000 with paired-end 59 bp × 59 bp reads. Sequencing data were demultiplexed using Illumina's BCL Convert and aligned to the Mus Musculus (mm10) reference sequence using DRAGEN RNA app on Basespace Sequence Hub (https://support-docs.illumina.com/SW/DRAGEN_v41/Content/SW/DRAGEN/TPipelineIntro_fDG.htm).

Differential expression analysis was done using DESeq2 R package[73]. A low-count filter was applied to remove genes with < 5 raw reads in > 75% of samples. Genes were normalized by variance stabilizing transformation and deemed to be differentially expressed when their Benjamini & Hochberg adjusted p-values were < 0.05. Gene Set Enrichment Analysis (GSEA) was done by the clusterProfiler

R package[74], using the MSigDB Hallmark gene set knowledgebase[75,76]. The sign of $\log_2$ fold change * ($-\log_{10}$ p-value) was used as the rank score in GSEA. The "tags" values of the GSEA output were plotted as "Gene Ratio", which is the ratio of the number of leading-edge genes (genes that drove the enrichment) to the total number of genes in each gene set. The results of differential expression or GSEA were plotted in a volcano plot or dot plot using ggplot2 R package[76]. The code for RNA-seq analyses is available at https://github.com/hcen/PDAC_InsrKO.

Proteomics analyses

The whole head of pancreata collected from female mice at 12 weeks of age (*Ptf1a*^{CreER};*Kras*$^{LSL-G12D}$;*Insr*$^{w/w}$;nTnG (n=3), *Ptf1a*^{CreER};*Kras*$^{LSL-G12D}$;*Insr*$^{w/f}$;nTnG (n=6), *Ptf1a*^{CreER};*Kras*$^{LSL-G12D}$;*Insr*$^{f/f}$;nTnG (n=6), *Ptf1a*^{CreER};*Insr*$^{w/w}$;nTnG (n=3), and *Ptf1a*^{CreER};*Insr*$^{f/f}$;nTnG (n=2) mice) were frozen and used for (phospho)proteomic analyses. The frozen sample was ground into powder in a liquid nitrogen-cooled mortar and pestle and kept on dry ice until mass-spec analysis. Proteins were extracted from cryopulverized tumors in a buffer containing 5% sodium dodecyl sulfate (SDS) and 100 mM TRIS pH 7.8 supplemented with PhosStop phosphatase inhibitor cocktail (Millipore-Sigma, part# 4906845001). The protein concentration of the lysate was determined using bicinchoninic acid assay (BCA) (Thermo Fisher Scientific, Waltham, MA, USA, part# 23225), and protein disulfide bonds were reduced and free Cysteines alkylated with 20 mM tris (2-carboxyethyl)phosphine (TCEP) and 30 mM iodoacetamide, respectively (Millipore-Sigma, part# 646547, and I1149 respectively). Proteolytic digestion of 250 µg of total protein was performed using S-TRAP Mini columns (Protifi LLC, Huntington NY, USA)[77]. Resultant tryptic peptides were then vacuum concentrated and desalted using Oasis HLB SPE cartridges (Waters, Milford, MA, USA, part# WAT094225). Peptides were vacuum concentrated and reconstituted in 0.1% trifluoro acetic acid (TFA), and 10% of the total sample was reserved for measurement of the total proteome. The remaining 90% of the sample was diluted in 80% acetonitrile with 0.1% TFA for automated phosphopeptide enrichment using AssayMap Fe-NTA (III) immobilized metal affinity chromatography (IMAC) cartridges and a Bravo liquid handling system using the phosphopeptide enrichment v 2.1 application (Agilent Technologies, Santa Clara, CA, USA, part# G5496-60085).

LC-MS/MS acquisition and data analysis

Samples for both total proteomics and phosphoproteomics were analyzed by data dependent acquisition (DDA) using an Easy-nLC 1200 and Q Exactive Plus (both Thermo Fisher Scientific, Waltham, MA, USA). Samples were first loaded onto a precolumn (Acclaim PepMap 100 C18, 3 µm particle size, 75 µm inner diameter x 2 cm) in 0.1% formic acid (buffer A), and gradient elution was performed using a 100-min method from 3 to 40% buffer B (84% acetonitrile, 0.1% formic acid) on the analytical column (Acclaim PepMap 100 C18, 2 µm particle size, 75 µm inner diameter x 25 cm) at a

flow rate of 300 nL/min. MS scans were acquired between 350-1,500 m/z at a resolution of 70,000, with an automatic gain control (AGC) target of 1 x 10e610E6 ions and a maximum injection time of 50 ms. The top 15 precursor ions with charge states +2, +, +3, and +4 were isolated with a window of 1.2 m/z, an AGC target of 2 x 10e410E4 and a maximum injection time of 64 ms and fragmented using a normalized collision energy (NCE) of 28. MS/MS were acquired at a resolution of 17,500 and the dynamic exclusion was set to 30 s. DDA MS raw data was processed with Proteome Discoverer 2.5 (Thermo Fisher Scientific, Waltham, MA, USA) and searched using Sequest HT against the mouse reference proteome FASTA database from Uniprot (downloaded October 1st 2021; 17,054 forward sequences). The enzyme specificity was set to trypsin with a maximum of 2 missed cleavages. Carbamidomethylation of cysteine was set as a fixed modification and oxidation of methionine, as well as phosphorylation of serine, threonine, and tyrosine as variable modifications. The precursor ion mass tolerance was set to 10 parts per million, and the product ion mass tolerance was set to 0.02 Da. Percolator was used to assess posterior error probabilities and the data was filtered using a false discovery rate (FDR) of <1% on peptide and protein level. The Minora node of Proteome Discoverer was used for label free quantitation. For the human comparison, Pathway enrichment was performed on our mouse data and PDAC human data[34] using Reactome (v80)[78]. We performed differential abundance analysis on the human data using the R package limma[79]. For our data, we used a cutoff of Adj. $p<0.05$. For the human data, we used Adj. $p<1^{-19}$ and 1^{-12} for the total proteins and phospho-proteins respectively to ensure a comparable proportion of the total number detected. The mass spectrometry proteomics data have been deposited to the ProteomeXchange Consortium via the PRIDE[80] partner repository with the dataset identifier PXD033845. All code is available at https://github.com/johnsonlabubc/PDAC-Insr-KO-Total-and-Phosphoproteomic-Analysis.

Primary mouse acinar cell isolation and three-dimensional culture

Primary pancreatic acinar cells were isolated from pancreata of wild-type female or male mice of the indicated mouse background fed normal chow diet (LabDiet Rodent Diet 20 Cat#5053) at the age of 6-8 weeks. *Ptf1a*^{CreER};*Insr*$^{f/f}$;nTnG mice and their control mice (*Ptf1a*^{CreER};*Insr*$^{w/w}$;nTnG) were given tamoxifen via subcutaneous injection two weeks prior to cell isolation. The acinar cell isolation procedure was adapted from the protocol described by Martinez and Storz[44]. Briefly, the mouse pancreas was harvested and washed three times in 1x HBSS and then minced into 1-5 mm pieces. The fragmented tissue was then digested with 5 mL (0.4 mg/mL) collagenase P solution (Sigma, Cat. No. 11213857001) in RPMI1640 (Sigma, Cat. No. R0883) at 37°C with gentle shaking for 18 minutes. HBSS (10 mL) with 5% FBS was added to terminate the digestion reaction, followed by 3 washes with 10 mL HBSS (5% FBS) to remove the residual collagenase P. After each wash, the tissue was pelleted (450g RCF, 2 min at room temperature) and the supernatant was removed. The digested tissue was resuspended in 10 mL HBSS (5% FBS) and filtered through a 100 µm cell strainer,

629 followed by a wash with 10 mL HBSS (5% FBS). The filtrate was gently added to 20 mL HBSS 30%
630 FBS cushion to form layers of cells. The cell mixture was centrifuged at 180g RCF at room
631 temperature for 2 minutes to pellet acinar cells. Appropriate number of acinar cells were then
632 resuspended in premade collagen solution (1 mg/ml rat tail type1 collagen (VWR, Cat. No.
633 CACB354236), 10x Waymouth's media (Cedarlane Labs, Cat. No. W1001-03), RPMI1640 complete
634 media (1% FBS, 1x penicillin/streptomycin (VWR, Cat. No. CA45000-650), 1 µg/mL dexamethasone
635 (Sigma, Cat. No. D2915), adjusted to pH = ~7.8 with 1 M NaOH) and plated (50 µL per well) in
636 collagen pre-coated 96-well plates. After solidification, 100 µL of the RPMI1640 complete media with
637 or without insulin (0.1 nM-100 nM) (Sigma, Cat. No. 11061-68-0), TGF-α (Fisher Scientific, Cat. No.
638 PHG005) (50ng/mL) or combined treatments, with or without 0.1 mg/mL soybean trypsin inhibitor
639 (Sigma, Cat. No. T9128) was added. *Ptf1a*^{CreER};*Insr*$^{f/f}$;nTnG acinar cells and the control cells were
640 cultured with Human plasma-like media (Gibco, Cat. No. A4899102), instead of RPMI1640, to ensure
641 the survival of *Insr*-deficient acinar cells. Media was replaced on day 1 and 3, and the numbers of
642 ADM events in each well were quantified on day 5. Isolated cells were maintained at 37°C in a
643 humidified incubator with 5% CO_2.
644
645 **QUANTIFICATION AND STATISTICAL ANALYSIS**
646 Animals were excluded from the histopathological analyses if they were found dead. Statistical
647 analyses were conducted with GraphPad Prism 9.3.0. The Shapiro-Wilk test was used to assess data
648 normality. One-way ANOVA was performed unless otherwise stated. Mixed-effect analyses were run
649 for glucose homeostasis data (mouse body weight, fasting glucose level, and fasting insulin level).
650 When comparing the histopathological measurements between male and female mice from the same
651 genotype, a two-tailed student's t-test was run for normally distributed data and a Mann-Whitney test
652 was performed for non-normally distributed data. Statistical parameters, including the exact value of
653 sample size n (animal number), precision measures and dispersion (mean ± SEM), and statistical
654 significance levels, are reported in the Figures and Figure legends. A p-value <0.05 was considered
655 significant. In Figures, asterisks denote statistical significance (*p<0.05, **p<0.01, ***p<0.001, and
656 ****p<0.0001).
657 For total proteomics data, normalization, imputation, and differential expression analyses were
658 performed on the protein abundances using Proteome Discoverer. Differential expression analysis
659 used background-based t-tests with p-values adjusted using Benjamini-Hochberg correction. The
660 proteins were filtered for significant comparisons (Adj. p<0.05), and heatmaps were created with
661 resultant protein lists. We also applied k-means clustering and extracted clusters with patterns of
662 interest[81]. From this heatmap, proteins were identified and values for all samples were plotted in a
663 heatmap and sorted with hierarchical clustering. We used STRING (v11) to generate an edge table
664 with differentially expressed total proteins (Adj. p<0.05) with an absolute log_2(Fold Change) cut-off of

2.5 in *Ptf1a*^{CreER};*Kras*$^{LSL\text{-}G12D}$;*Insr*$^{w/w}$;nTnG compared to *Ptf1a*^{CreER};*Kras*$^{LSL\text{-}G12D}$;*Insr*$^{f/f}$;nTnG. Protein-protein relationships were only included if they involved experimental evidence or interactions annotated in other databases[35]. Cytoscape (v3.9.1) was used to visualize the network[82], with background images created with BioRender.com.

Phospho-proteomics data were analyzed two ways. In the first approach, we only used phospho-peptides with measurements made in a minimum of 2/3 of all the samples and at least one sample per group. We imputed missing phospho-protein values in samples before normalization and statistical analysis using the same process as the total proteomics, allowing a broader assessment of the phospho-protein landscape. These were plotted using volcano plots and against the corresponding proteins in the total protein data set with calculated $\log_2$(Fold Change) of the median. In the second approach, we aggregated the abundances of each sample for each phospho-site detected, and normalized each of the detected phospho-sites to the total abundance of the corresponding protein. We only included phospho-sites where every sample had an experimentally measured total protein value. The second method used differential expression analysis performed using the R package limma on the *Ptf1a*^{CreER};*Kras*$^{LSL\text{-}G12D}$;*Insr*$^{w/w}$;nTnG versus *Ptf1a*^{CreER};*Kras*$^{LSL\text{-}G12D}$;*Insr*$^{f/f}$;nTnG comparison[79]. Phosphosite[39] was used to determine upstream activators, cellular location, and function of each protein, as well as the specific kinases of the detected phospho-sites, if known. STRING was used to identify proteins that interact with each other[35].

References

1. Rahib, L., Smith, B.D., Aizenberg, R., Rosenzweig, A.B., Fleshman, J.M., and Matrisian, L.M. (2014). Projecting cancer incidence and deaths to 2030: the unexpected burden of thyroid, liver, and pancreas cancers in the United States. Cancer Res *74*, 2913-2921. 10.1158/0008-5472.CAN-14-0155.
2. Ilic, M., and Ilic, I. (2016). Epidemiology of pancreatic cancer. World J Gastroenterol *22*, 9694-9705. 10.3748/wjg.v22.i44.9694.
3. Gallagher, E.J., and LeRoith, D. (2020). Hyperinsulinaemia in cancer. Nat Rev Cancer *20*, 629-644. 10.1038/s41568-020-0295-5.
4. Zhang, A.M.Y., Wellberg, E.A., Kopp, J.L., and Johnson, J.D. (2021). Hyperinsulinemia in Obesity, Inflammation, and Cancer. Diabetes Metab J *45*, 285-311. 10.4093/dmj.2020.0250.
5. Stolzenberg-Solomon, R.Z., Graubard, B.I., Chari, S., Limburg, P., Taylor, P.R., Virtamo, J., and Albanes, D. (2005). Insulin, glucose, insulin resistance, and pancreatic cancer in male smokers. JAMA *294*, 2872-2878. 10.1001/jama.294.22.2872.
6. Pisani, P. (2008). Hyper-insulinaemia and cancer, meta-analyses of epidemiological studies. Arch Physiol Biochem *114*, 63-70. 10.1080/13813450801954451.
7. Dawson, D.W., Hertzer, K., Moro, A., Donald, G., Chang, H.H., Go, V.L., Pandol, S.J., Lugea, A., Gukovskaya, A.S., Li, G., et al. (2013). High-fat, high-calorie diet promotes early pancreatic neoplasia in the conditional KrasG12D mouse model. Cancer Prev Res (Phila) *6*, 1064-1073. 10.1158/1940-6207.CAPR-13-0065.
8. Chang, H.H., Moro, A., Takakura, K., Su, H.Y., Mo, A., Nakanishi, M., Waldron, R.T., French, S.W., Dawson, D.W., Hines, O.J., et al. (2017). Incidence of pancreatic cancer is dramatically increased by a high fat, high calorie diet in KrasG12D mice. PLoS One *12*, e0184455. 10.1371/journal.pone.0184455.
9. Zhang, A.M.Y., Magrill, J., de Winter, T.J.J., Hu, X., Skovso, S., Schaeffer, D.F., Kopp, J.L., and Johnson, J.D. (2019). Endogenous Hyperinsulinemia Contributes to Pancreatic Cancer Development. Cell Metab *30*, 403-404. 10.1016/j.cmet.2019.07.003.
10. Zhang, A.M.Y., Chu, K.H., Daly, B.F., Ruiter, T., Dou, Y., Yang, J.C.C., de Winter, T.J.J., Chhuor, J., Wang, S., Flibotte, S., et al. (2022). Effects of hyperinsulinemia on pancreatic cancer development and the immune microenvironment revealed through single-cell transcriptomics. Cancer Metab *10*, 5. 10.1186/s40170-022-00282-z.
11. Mehran, A.E., Templeman, N.M., Brigidi, G.S., Lim, G.E., Chu, K.Y., Hu, X., Botezelli, J.D., Asadi, A., Hoffman, B.G., Kieffer, T.J., et al. (2012). Hyperinsulinemia drives diet-induced obesity independently of brain insulin production. Cell Metab *16*, 723-737. 10.1016/j.cmet.2012.10.019.
12. Templeman, N.M., Flibotte, S., Chik, J.H.L., Sinha, S., Lim, G.E., Foster, L.J., Nislow, C., and Johnson, J.D. (2017). Reduced Circulating Insulin Enhances Insulin Sensitivity in Old Mice and Extends Lifespan. Cell Rep *20*, 451-463. 10.1016/j.celrep.2017.06.048.
13. Templeman, N.M., Clee, S.M., and Johnson, J.D. (2015). Suppression of hyperinsulinaemia in growing female mice provides long-term protection against obesity. Diabetologia *58*, 2392-2402. 10.1007/s00125-015-3676-7.
14. Chan, D.S., Vieira, A.R., Aune, D., Bandera, E.V., Greenwood, D.C., McTiernan, A., Navarro Rosenblatt, D., Thune, I., Vieira, R., and Norat, T. (2014). Body mass index and survival in women with breast cancer-systematic literature review and meta-analysis of 82 follow-up studies. Ann Oncol *25*, 1901-1914. 10.1093/annonc/mdu042.
15. Waters, A.M., and Der, C.J. (2018). KRAS: The Critical Driver and Therapeutic Target for Pancreatic Cancer. Cold Spring Harb Perspect Med *8*. 10.1101/cshperspect.a031435.
16. Heestand, G.M., and Kurzrock, R. (2015). Molecular landscape of pancreatic cancer: implications for current clinical trials. Oncotarget *6*, 4553-4561. 10.18632/oncotarget.2972.
17. Janku, F., Wheler, J.J., Naing, A., Falchook, G.S., Hong, D.S., Stepanek, V.M., Fu, S., Piha-Paul, S.A., Lee, J.J., Luthra, R., et al. (2013). PIK3CA mutation H1047R is associated with response to PI3K/AKT/mTOR signaling pathway inhibitors in early-phase clinical trials. Cancer Res *73*, 276-284. 10.1158/0008-5472.CAN-12-1726.

18. Payne, S.N., Maher, M.E., Tran, N.H., Van De Hey, D.R., Foley, T.M., Yueh, A.E., Leystra, A.A., Pasch, C.A., Jeffrey, J.J., Clipson, L., et al. (2015). PIK3CA mutations can initiate pancreatic tumorigenesis and are targetable with PI3K inhibitors. Oncogenesis *4*, e169. 10.1038/oncsis.2015.28.
19. Sivaram, N., McLaughlin, P.A., Han, H.V., Petrenko, O., Jiang, Y.P., Ballou, L.M., Pham, K., Liu, C., van der Velden, A.W., and Lin, R.Z. (2019). Tumor-intrinsic PIK3CA represses tumor immunogenecity in a model of pancreatic cancer. J Clin Invest *129*, 3264-3276. 10.1172/JCI123540.
20. Hopkins, B.D., Pauli, C., Du, X., Wang, D.G., Li, X., Wu, D., Amadiume, S.C., Goncalves, M.D., Hodakoski, C., Lundquist, M.R., et al. (2018). Suppression of insulin feedback enhances the efficacy of PI3K inhibitors. Nature *560*, 499-503. 10.1038/s41586-018-0343-4.
21. Belfiore, A., Malaguarnera, R., Vella, V., Lawrence, M.C., Sciacca, L., Frasca, F., Morrione, A., and Vigneri, R. (2017). Insulin Receptor Isoforms in Physiology and Disease: An Updated View. Endocr Rev *38*, 379-431. 10.1210/er.2017-00073.
22. Aljada, A., Saleh, A.M., Al-Aqeel, S.M., Shamsa, H.B., Al-Bawab, A., Al Dubayee, M., and Ahmed, A.A. (2015). Quantification of insulin receptor mRNA splice variants as a diagnostic tumor marker in breast cancer. Cancer Biomark *15*, 653-661. 10.3233/CBM-150505.
23. Law, J.H., Habibi, G., Hu, K., Masoudi, H., Wang, M.Y., Stratford, A.L., Park, E., Gee, J.M., Finlay, P., Jones, H.E., et al. (2008). Phosphorylated insulin-like growth factor-i/insulin receptor is present in all breast cancer subtypes and is related to poor survival. Cancer Res *68*, 10238-10246. 10.1158/0008-5472.CAN-08-2755.
24. Kopp, J.L., von Figura, G., Mayes, E., Liu, F.F., Dubois, C.L., Morris, J.P.t., Pan, F.C., Akiyama, H., Wright, C.V., Jensen, K., et al. (2012). Identification of Sox9-dependent acinar-to-ductal reprogramming as the principal mechanism for initiation of pancreatic ductal adenocarcinoma. Cancer Cell *22*, 737-750. 10.1016/j.ccr.2012.10.025.
25. Muzumdar, M.D., Tasic, B., Miyamichi, K., Li, L., and Luo, L. (2007). A global double-fluorescent Cre reporter mouse. Genesis *45*, 593-605. 10.1002/dvg.20335.
26. Khasawneh, J., Schulz, M.D., Walch, A., Rozman, J., Hrabe de Angelis, M., Klingenspor, M., Buck, A., Schwaiger, M., Saur, D., Schmid, R.M., et al. (2009). Inflammation and mitochondrial fatty acid beta-oxidation link obesity to early tumor promotion. Proc Natl Acad Sci U S A *106*, 3354-3359. 10.1073/pnas.0802864106.
27. Lumeng, C.N., and Saltiel, A.R. (2011). Inflammatory links between obesity and metabolic disease. J Clin Invest *121*, 2111-2117. 10.1172/JCI57132.
28. Berglund, E.D., Li, C.Y., Poffenberger, G., Ayala, J.E., Fueger, P.T., Willis, S.E., Jewell, M.M., Powers, A.C., and Wasserman, D.H. (2008). Glucose metabolism in vivo in four commonly used inbred mouse strains. Diabetes *57*, 1790-1799. 10.2337/db07-1615.
29. Collins, M.A., Bednar, F., Zhang, Y., Brisset, J.C., Galban, S., Galban, C.J., Rakshit, S., Flannagan, K.S., Adsay, N.V., and Pasca di Magliano, M. (2012). Oncogenic Kras is required for both the initiation and maintenance of pancreatic cancer in mice. J Clin Invest *122*, 639-653. 10.1172/JCI59227.
30. Chen, Z., Downing, S., and Tzanakakis, E.S. (2019). Four Decades After the Discovery of Regenerating Islet-Derived (Reg) Proteins: Current Understanding and Challenges. Front Cell Dev Biol *7*, 235. 10.3389/fcell.2019.00235.
31. Li, Q., Wang, H., Zogopoulos, G., Shao, Q., Dong, K., Lv, F., Nwilati, K., Gui, X.Y., Cuggia, A., Liu, J.L., and Gao, Z.H. (2016). Reg proteins promote acinar-to-ductal metaplasia and act as novel diagnostic and prognostic markers in pancreatic ductal adenocarcinoma. Oncotarget *7*, 77838-77853. 10.18632/oncotarget.12834.
32. Steiner, S., Seleznik, G.M., Reding, T., Stopic, M., Lenggenhager, D., Ten Buren, E., Eshmuminov, D., Endhardt, K., Hagedorn, C., Heidenblut, A.M., et al. (2022). De novo expression of gastrokines in pancreatic precursor lesions impede the development of pancreatic cancer. Oncogene *41*, 1507-1517. 10.1038/s41388-022-02182-4.
33. Dumartin, L., Alrawashdeh, W., Trabulo, S.M., Radon, T.P., Steiger, K., Feakins, R.M., di Magliano, M.P., Heeschen, C., Esposito, I., Lemoine, N.R., and Crnogorac-Jurcevic, T. (2017).

ER stress protein AGR2 precedes and is involved in the regulation of pancreatic cancer initiation. Oncogene *36*, 3094-3103. 10.1038/onc.2016.459.

34. Cao, L., Huang, C., Cui Zhou, D., Hu, Y., Lih, T.M., Savage, S.R., Krug, K., Clark, D.J., Schnaubelt, M., Chen, L., et al. (2021). Proteogenomic characterization of pancreatic ductal adenocarcinoma. Cell *184*, 5031-5052 e5026. 10.1016/j.cell.2021.08.023.
35. Szklarczyk, D., Gable, A.L., Nastou, K.C., Lyon, D., Kirsch, R., Pyysalo, S., Doncheva, N.T., Legeay, M., Fang, T., Bork, P., et al. (2021). The STRING database in 2021: customizable protein-protein networks, and functional characterization of user-uploaded gene/measurement sets. Nucleic Acids Res *49*, D605-D612. 10.1093/nar/gkaa1074.
36. Binder, J.X., Pletscher-Frankild, S., Tsafou, K., Stolte, C., O'Donoghue, S.I., Schneider, R., and Jensen, L.J. (2014). COMPARTMENTS: unification and visualization of protein subcellular localization evidence. Database (Oxford) *2014*, bau012. 10.1093/database/bau012.
37. Hernandez, V.J., Weng, J., Ly, P., Pompey, S., Dong, H., Mishra, L., Schwarz, M., Anderson, R.G., and Michaely, P. (2013). Cavin-3 dictates the balance between ERK and Akt signaling. Elife *2*, e00905. 10.7554/eLife.00905.
38. Haoning Howard Cen, J.R., Libin Abraham, Michael R. Gold, Leonard J. Foster, James D. Johnson (2022). Insulin-dependent and -independent dynamics of insulin receptor trafficking in muscle cells. bioRxiv.
39. Hornbeck, P.V., Zhang, B., Murray, B., Kornhauser, J.M., Latham, V., and Skrzypek, E. (2015). PhosphoSitePlus, 2014: mutations, PTMs and recalibrations. Nucleic Acids Res *43*, D512-520. 10.1093/nar/gku1267.
40. Hong, S., Freeberg, M.A., Han, T., Kamath, A., Yao, Y., Fukuda, T., Suzuki, T., Kim, J.K., and Inoki, K. (2017). LARP1 functions as a molecular switch for mTORC1-mediated translation of an essential class of mRNAs. Elife *6*. 10.7554/eLife.25237.
41. Rao, R.V., Holicky, E.L., Kuntz, S.M., and Miller, L.J. (2000). CCK receptor phosphorylation exposes regulatory domains affecting phosphorylation and receptor trafficking. Am J Physiol Cell Physiol *279*, C1986-1992. 10.1152/ajpcell.2000.279.6.C1986.
42. Smith, J.P., and Solomon, T.E. (2014). Cholecystokinin and pancreatic cancer: the chicken or the egg? Am J Physiol Gastrointest Liver Physiol *306*, G91-G101. 10.1152/ajpgi.00301.2013.
43. Means, A.L., Meszoely, I.M., Suzuki, K., Miyamoto, Y., Rustgi, A.K., Coffey, R.J., Jr., Wright, C.V., Stoffers, D.A., and Leach, S.D. (2005). Pancreatic epithelial plasticity mediated by acinar cell transdifferentiation and generation of nestin-positive intermediates. Development *132*, 3767-3776. dev.01925 [pii]10.1242/dev.01925.
44. Fleming Martinez, A.K., and Storz, P. (2019). Mimicking and Manipulating Pancreatic Acinar-to-Ductal Metaplasia in 3-dimensional Cell Culture. J Vis Exp. 10.3791/59096.
45. Means, A.L., Meszoely, I.M., Suzuki, K., Miyamoto, Y., Rustgi, A.K., Coffey, R.J., Wright, C.V.E., Stoffers, D.A., and Leach, S.D. (2005). Pancreatic epithelial plasticity mediated by acinar cell transdifferentiation and generation of nestin-positive intermediates. Development (Cambridge, England) *132*, 3767-3776. 10.1242/dev.01925.
46. Turner, S., and Lundeen, T.F. (1987). Two case reports. TMJ Update *5*, 45-49.
47. Morris, J.P., Cano, D.A., Sekine, S., Wang, S.C., and Hebrok, M. (2010). Beta-catenin blocks Kras-dependent reprogramming of acini into pancreatic cancer precursor lesions in mice. J Clin Invest *120*, 508-520. 10.1172/JCI40045.
48. Cherrington, A.D. (2005). The role of hepatic insulin receptors in the regulation of glucose production. J Clin Invest *115*, 1136-1139. 10.1172/JCI25152.
49. Haeusler, R.A., McGraw, T.E., and Accili, D. (2018). Biochemical and cellular properties of insulin receptor signalling. Nat Rev Mol Cell Biol *19*, 31-44. 10.1038/nrm.2017.89.
50. Cen, H.H., Hussein, B., Botezelli, J.D., Wang, S., Zhang, J.A., Noursadeghi, N., Jessen, N., Rodrigues, B., Timmons, J.A., and Johnson, J.D. (2022). Human and mouse muscle transcriptomic analyses identify insulin receptor mRNA downregulation in hyperinsulinemia-associated insulin resistance. FASEB J *36*, e22088. 10.1096/fj.202100497RR.
51. Sato, K., Hikita, H., Myojin, Y., Fukumoto, K., Murai, K., Sakane, S., Tamura, T., Yamai, T., Nozaki, Y., Yoshioka, T., et al. (2020). Hyperglycemia enhances pancreatic cancer progression

accompanied by elevations in phosphorylated STAT3 and MYC levels. PloS one *15*, e0235573-e0235573. 10.1371/journal.pone.0235573.

52. Vaziri-Gohar, A., Hue, J.J., Graor, H.G., Abbas, A., Zarei, M., Hajihassani, O., Titomihelakis, G., Feczko, J., Rathore, M., Wang, R., et al. (2022). Increased glucose availability sensitizes pancreatic cancer to chemotherapy. bioRxiv, 2022.2004.2029.490090. 10.1101/2022.04.29.490090.
53. Samuels, Y., Wang, Z., Bardelli, A., Silliman, N., Ptak, J., Szabo, S., Yan, H., Gazdar, A., Powell, S.M., Riggins, G.J., et al. (2004). High frequency of mutations of the PIK3CA gene in human cancers. Science *304*, 554. 10.1126/science.1096502.
54. Yang, J., Nie, J., Ma, X., Wei, Y., Peng, Y., and Wei, X. (2019). Targeting PI3K in cancer: mechanisms and advances in clinical trials. Mol Cancer *18*, 26. 10.1186/s12943-019-0954-x.
55. Guo, Y.J., Pan, W.W., Liu, S.B., Shen, Z.F., Xu, Y., and Hu, L.L. (2020). ERK/MAPK signalling pathway and tumorigenesis. Exp Ther Med *19*, 1997-2007. 10.3892/etm.2020.8454.
56. Godsland, I.F. (2009). Insulin resistance and hyperinsulinaemia in the development and progression of cancer. Clin Sci (Lond) *118*, 315-332. 10.1042/CS20090399.
57. Chan, M.T., Lim, G.E., Skovso, S., Yang, Y.H., Albrecht, T., Alejandro, E.U., Hoesli, C.A., Piret, J.M., Warnock, G.L., and Johnson, J.D. (2014). Effects of insulin on human pancreatic cancer progression modeled in vitro. BMC Cancer *14*, 814. 10.1186/1471-2407-14-814.
58. Henderson, J.R., Daniel, P.M., and Fraser, P.A. (1981). The pancreas as a single organ: the influence of the endocrine upon the exocrine part of the gland. Gut *22*, 158-167. 10.1136/gut.22.2.158.
59. Soling, H.D., and Unger, K.O. (1972). The role of insulin in the regulation of -amylase synthesis in the rat pancreas. Eur J Clin Invest *2*, 199-212. 10.1111/j.1365-2362.1972.tb00645.x.
60. Frier, B.M., Saunders, J.H., Wormsley, K.G., and Bouchier, I.A. (1976). Exocrine pancreatic function in juvenile-onset diabetes mellitus. Gut *17*, 685-691. 10.1136/gut.17.9.685.
61. Guerra, C., Schuhmacher, A.J., Canamero, M., Grippo, P.J., Verdaguer, L., Perez-Gallego, L., Dubus, P., Sandgren, E.P., and Barbacid, M. (2007). Chronic pancreatitis is essential for induction of pancreatic ductal adenocarcinoma by K-Ras oncogenes in adult mice. Cancer Cell *11*, 291-302. 10.1016/j.ccr.2007.01.012.
62. Otsuki, M. (2000). Pathophysiological role of cholecystokinin in humans. J Gastroenterol Hepatol *15 Suppl*, D71-83. 10.1046/j.1440-1746.2000.02178.x.
63. Varga, G., Papp, M., Solomon, T.E., Scarpignato, C., Toth, I.E., and Szabo, D. (1988). Caerulein in supramaximal doses fails to stimulate pancreatic growth, but it forces secretory granulopoiesis. Acta Physiol Hung *71*, 99-106.
64. Dembinski, A.B., and Johnson, L.R. (1980). Stimulation of Pancreatic Growth by Secretin, Caerulein, and Pentagastrin. Endocrinology *106*, 323-328. 10.1210/endo-106-1-323.
65. Incio, J., Liu, H., Suboj, P., Chin, S.M., Chen, I.X., Pinter, M., Ng, M.R., Nia, H.T., Grahovac, J., Kao, S., et al. (2016). Obesity-Induced Inflammation and Desmoplasia Promote Pancreatic Cancer Progression and Resistance to Chemotherapy. Cancer Discov *6*, 852-869. 10.1158/2159-8290.CD-15-1177.
66. Bruce, J.I.E., Sanchez-Alvarez, R., Sans, M.D., Sugden, S.A., Qi, N., James, A.D., and Williams, J.A. (2021). Insulin protects acinar cells during pancreatitis by preserving glycolytic ATP supply to calcium pumps. Nat Commun *12*, 4386. 10.1038/s41467-021-24506-w.
67. Pan, F.C., Bankaitis, E.D., Boyer, D., Xu, X., Van de Casteele, M., Magnuson, M.A., Heimberg, H., and Wright, C.V. (2013). Spatiotemporal patterns of multipotentiality in Ptf1a-expressing cells during pancreas organogenesis and injury-induced facultative restoration. Development *140*, 751-764. 10.1242/dev.090159.
68. Skovso, S., Panzhinskiy, E., Kolic, J., Cen, H.H., Dionne, D.A., Dai, X.Q., Sharma, R.B., Elghazi, L., Ellis, C.E., Faulkner, K., et al. (2022). Beta-cell specific Insr deletion promotes insulin hypersecretion and improves glucose tolerance prior to global insulin resistance. Nat Commun *13*, 735. 10.1038/s41467-022-28039-8.

69. Tuveson, D.A., Shaw, A.T., Willis, N.A., Silver, D.P., Jackson, E.L., Chang, S., Mercer, K.L., Grochow, R., Hock, H., Crowley, D., et al. (2004). Endogenous oncogenic K-ras(G12D) stimulates proliferation and widespread neoplastic and developmental defects. Cancer Cell *5*, 375-387.
70. Prigge, J.R., Wiley, J.A., Talago, E.A., Young, E.M., Johns, L.L., Kundert, J.A., Sonsteng, K.M., Halford, W.P., Capecchi, M.R., and Schmidt, E.E. (2013). Nuclear double-fluorescent reporter for in vivo and ex vivo analyses of biological transitions in mouse nuclei. Mamm Genome. 10.1007/s00335-013-9469-8.
71. Bruning, J.C., Michael, M.D., Winnay, J.N., Hayashi, T., Horsch, D., Accili, D., Goodyear, L.J., and Kahn, C.R. (1998). A muscle-specific insulin receptor knockout exhibits features of the metabolic syndrome of NIDDM without altering glucose tolerance. Mol Cell *2*, 559-569. 10.1016/s1097-2765(00)80155-0.
72. Lee, A.Y.L., Dubois, C.L., Sarai, K., Zarei, S., Schaeffer, D.F., Sander, M., and Kopp, J.L. (2018). Cell of origin affects tumour development and phenotype in pancreatic ductal adenocarcinoma. Gut. 10.1136/gutjnl-2017-314426.
73. Love, M.I., Huber, W., and Anders, S. (2014). Moderated estimation of fold change and dispersion for RNA-seq data with DESeq2. Genome Biol *15*, 550. 10.1186/s13059-014-0550-8.
74. Yu, G., Wang, L.G., Han, Y., and He, Q.Y. (2012). clusterProfiler: an R package for comparing biological themes among gene clusters. OMICS *16*, 284-287. 10.1089/omi.2011.0118.
75. Liberzon, A., Birger, C., Thorvaldsdóttir, H., Ghandi, M., Mesirov, J.P., and Tamayo, P. (2015). The Molecular Signatures Database (MSigDB) hallmark gene set collection. Cell Syst *1*, 417-425. 10.1016/j.cels.2015.12.004.
76. Wickham, H. (2016). ggplot2: Elegant Graphics for Data Analysis (Springer-Verlag New York).
77. HaileMariam, M., Eguez, R.V., Singh, H., Bekele, S., Ameni, G., Pieper, R., and Yu, Y. (2018). S-Trap, an Ultrafast Sample-Preparation Approach for Shotgun Proteomics. J Proteome Res *17*, 2917-2924. 10.1021/acs.jproteome.8b00505.
78. Gillespie, M., Jassal, B., Stephan, R., Milacic, M., Rothfels, K., Senff-Ribeiro, A., Griss, J., Sevilla, C., Matthews, L., Gong, C., et al. (2022). The reactome pathway knowledgebase 2022. Nucleic Acids Res *50*, D687-D692. 10.1093/nar/gkab1028.
79. Ritchie, M.E., Phipson, B., Wu, D., Hu, Y., Law, C.W., Shi, W., and Smyth, G.K. (2015). limma powers differential expression analyses for RNA-sequencing and microarray studies. Nucleic Acids Res *43*, e47. 10.1093/nar/gkv007.
80. Perez-Riverol, Y., Bai, J., Bandla, C., Garcia-Seisdedos, D., Hewapathirana, S., Kamatchinathan, S., Kundu, D.J., Prakash, A., Frericks-Zipper, A., Eisenacher, M., et al. (2022). The PRIDE database resources in 2022: a hub for mass spectrometry-based proteomics evidences. Nucleic Acids Res *50*, D543-D552. 10.1093/nar/gkab1038.
81. Gu, Z., Eils, R., and Schlesner, M. (2016). Complex heatmaps reveal patterns and correlations in multidimensional genomic data. Bioinformatics *32*, 2847-2849. 10.1093/bioinformatics/btw313.
82. Shannon, P., Markiel, A., Ozier, O., Baliga, N.S., Wang, J.T., Ramage, D., Amin, N., Schwikowski, B., and Ideker, T. (2003). Cytoscape: a software environment for integrated models of biomolecular interaction networks. Genome Res *13*, 2498-2504. 10.1101/gr.1239303.

Figure Legends

Fig. 1. Loss of *Insr* in pancreatic acinar cells had no effect on glucose homeostasis and pancreas size.

A, Schematic describing a mouse model designed to test the role of insulin receptor signaling on HFD-accelerated PDAC initiation. On the background of the *Ptf1a*^{CreER} mice, we generated mice having two wild-type *Insr* alleles (*Ptf1a*^{CreER};*Insr*$^{w/w}$;nTnG) or two *Insr* floxed alleles (*Ptf1a*^{CreER};*Insr*$^{f/f}$;nTnG). On the background of the *Ptf1a*^{CreER}-induced *Kras*^{G12D} pancreatic cancer model with the nTnG lineage allele (PK), we generated mice having two wild-type *Insr* alleles (PK-*Insr*$^{w/w}$), one *Insr* floxed allele (PK-*Insr*$^{w/f}$), or two *Insr* floxed alleles (PK-*Insr*$^{f/f}$). Both male (M:, circles) and (F:, triangles) mice were analyzed. **B**, Three-week-old mice were weaned and provided high fat diet (HFD) for the duration of the study. At 4-weeks-old, they were injected with tamoxifen (TM) on 3 consecutive days. Physiological measures were taken every 3 months for 10 months, mice were euthanized at 12 or 43.5 weeks of age for histopathology. The mice which were euthanized at 12 weeks of age were also used for proteomics, phospho-proteomics and RNA-sequencing analyses. **C-H,** Body weight (**C-D**), fasting blood glucose (**E-F**), and fasting insulin (**G-H**) measurements in male (**C, E, G**) and female (**D, F, H**) *Ptf1a*^{CreER}-*Insr*$^{w/w}$;nTnG and *Ptf1a*^{CreER}-*Insr*$^{f/f}$;nTnG mice measured over 57 weeks (n= 10-17) or PK-*Insr*$^{w/w}$, PK-*Insr*$^{w/f}$, and PK-*Insr*$^{f/f}$ mice up to 43.5 weeks (n= 13-33). Values shown as mean ± SEM. *p<0.05.

Fig. 2. Loss of *Insr* in acinar cells reduced PanIN and PDAC formation.

A, Percentage of mice of the indicated genotype that were found dead or reached humane endpoint throughout the study. The star symbol indicates whether a macroscopic mass was observed in the pancreas at necropsy, when possible. There were 9 PK-*Insr*$^{w/w}$, 13 PK-*Insr*$^{w/f}$, and 6 PK-*Insr*$^{f/f}$ male mice and 9 PK-*Insr*$^{w/w}$ 17 PK-*Insr*$^{w/f}$, and 9 PK-*Insr*$^{f/f}$ female mice in the cohort. At 43.5 weeks, the remaining mice were euthanized and assessed for presence of tumors. **B,** The number of mice dead before or at 43 weeks with or without tumor presence. **C-D,** Representative whole section (top) and high-magnification (bottom) H&E images of pancreatic slides from 43.5-week-old male (**C**) and female (**D**) PK-*Insr*$^{w/w}$, PK-*Insr*$^{w/f}$, and PK-*Insr*$^{f/f}$ mice. **E-H,** Quantification of acinar cell area (**E**)**,** PanIN plus tumor area (**F**), PanIN only area (**G**), or tumor area (**H**) in pancreata from each genotype and sex (male or female) at 43.5 weeks of age (n= 5-16). (**F**) Filled circles or triangles denote mice that developed tumors. Scale bars: 2 mm (**C-D,** top) and 0.1mm (**C-D**, bottom). Values are shown as mean ± SEM. *p<0.05, **p<0.01, ***p<0.001.

Fig. 3. Loss of *Insr* in acinar cells reduced PanIN lesions initiation.

A-B, Representative whole section (top) and high-magnification (bottom) H&E images of pancreatic slides from 12-week-old male (**A**) and female (**B**) PK-*Insr*$^{w/w}$, PK-*Insr*$^{w/f}$, and PK-*Insr*$^{f/f}$ mice. **C,**

Quantification of PanIN area in 12-week-old pancreata from each genotype and sex (male or female) (n= 3-14). The difference in PanIN formation between male and female PK-*Insr*$^{w/w}$ mice was not significantly different. **D**, Volcano plot for genes that were significantly up- or down-regulated in PK-*Insr*$^{f/f}$ mice (n=4) compared to PK-*Insr*$^{w/w}$ mice (n=4). **E,** Gene set enrichment analysis for genes differentially expressed between PK-*Insr*$^{f/f}$ mice and PK-*Insr*$^{w/w}$ mice. Scale bars: 2 mm (top) and 0.1mm (bottom). Values are shown as mean ± SEM. *p<0.05, **p<0.01.

Fig. 4. The proteomic analysis of insulin receptors' effects on PanIN initiation.

A, Volcano plot for proteins that were significantly up- or down-regulated in PK-*Insr*$^{w/w}$ mice (n=3) compared to *Ptf1a*^{CreER};*Insr*$^{w/w}$;nTnG mice (n=3). **B**, Volcano plot for proteins that were significantly up- or down-regulated in *Ptf1a*^{CreER};*Insr*$^{f/f}$;nTnG mice (n=2) compared to *Ptf1a*^{CreER};*Insr*$^{w/w}$;nTnG mice (n=3). **C**, Volcano plot showing proteins that were significantly up- or down-regulated in PK-*Insr*$^{f/f}$ mice (n=6) compared to PK-*Insr*$^{w/w}$ mice (n=3). **D,** Proteins that were differentially abundant between PK-*Insr*$^{w/w}$ and PK-*Insr*$^{f/f}$ mice were selected and their average abundance across all genotypes was used for k-means clustering. The clusters were visualized by heatmap to show their variance across all genotypes and samples. The proteins in clusters 1, 2, 3, and 7 are listed in the order shown in the heatmap from top to bottom. This information can also be found in the Supplemental Table S4 Clusters 1-8.

Fig. 5. Loss of *Insr* in acinar cells reduced digestive enzymes production in pancreas.

A, Differentially abundant proteins between PK-*Insr*$^{w/w}$ and PK-*Insr*$^{f/f}$ pancreata were connected using STRING and diagrammatically presented here in the context of Insr signaling and cellular organelles and functions (outline created in Biorender). The color in each oval reflects the fold change, while the thickness of the line around the oval represents the Adj. p-value. Proteins depicted in white ovals were added to show the potential relationship of the differentially abundant proteins to insulin signaling. **B**, Heatmap showing the change of protein abundance between genotypes for proteins involved in pancreatic digestive enzymes secretion. **C**, The percentage of summed digestive enzyme abundances in total measured proteins for each genotype. Values are shown as mean ± SEM. **p<0.01.

Fig. 6. The phospho-proteomic analysis of insulin receptors' effects on PanIN initiation.

A, Volcano plots for proteins with phosphor-sites that were significantly up or down regulated in PK-*Insr*$^{f/f}$ mice compared to PK-*Insr*$^{w/w}$ mice. **B**, Change in phospho-peptide abundance (Adj. p-values indicated in red) compared to the change in corresponding protein's abundance between PK-*Insr*$^{f/f}$ mice and PK-*Insr*$^{w/w}$ mice. **C**, TOP: Schematic of phosphorylation sites on Cckar that were differentially abundant in any comparison. BOTTOM: The relative phospho-peptide abundance (arbitrary units) for each detected phospho-peptide for all samples and genotypes. **D,** Intracellular

locations (outline created in Biorender) and functions of differentially abundant phospho-sites and their corresponding protein. The color in each attached phospho-site reflects the fold change, while the thickness of the border represents the Adj. p-value. Values are shown as mean ± SEM. *p<0.05, **p<0.01, ***p<0.001, ****p<0.0001.

Fig. 7. Insulin receptor signaling promotes PanIN initiation via increased inflammation associated with hyperactive digestive enzyme production.

A-B, Representative whole section (top) and high-magnification (bottom) images of pancreatic slides stained with Sirius red from 12-week-old male (**A**) and female (**B**) PK-*Insr*$^{w/w}$, PK-*Insr*$^{w/f}$, and PK-*Insr*$^{f/f}$ mice. **C,** Quantification of Sirius red positive area for mice from each genotype and sex (male (M:) or female (F:)) (n= 4-9). **D,** Schematic of the experimental design of the ADM formation assay using 3D acinar cell explant system. **E,** Representative bright field images of acinar cell clusters and duct formation (ring structures) on day 5 of treatment with or without 50 ng/mL TGF-α or 100 nM insulin in the absence of trypsin inhibitor. ADM structures are indicated by red arrows. **F,** Quantification of the fold change in ADM events in primary mouse acinar cell 3D explants (CD1 female) after 5 days of treatment with a combination of ± TGF-α and ± insulin and ± soybean trypsin inhibitor. (n = 4 independent experiments, two-way ANOVA). Fold change values were calculated as treatment/negative control (no insulin or TGF-α or trypsin inhibitor) for each experiment. **G,** Quantification of ADM transformation rate of all acini clusters per well. Acinar clusters were isolated from female *Ptf1a*^{CreER};*Insr*$^{w/w}$;nTnG (n=3) or *Ptf1a*^{CreER};*Insr*$^{f/f}$;nTnG (n=4) mice. Acinar cell 3D explants were quantified after 5 days treatment with a combination of ± TGF-α and ± insulin with and without soybean trypsin inhibitor. **H.** Schematic demonstrating obesity or diet-induced hyperinsulinemia, via Insr, promoted PanIN formation through increasing digestive enzymes production/release and its associated inflammation. Scale bars: 2 mm (**A**, **B**; top), 0.1 mm (**A**, **B**; bottom), and 100µm (**E**). Values are shown as mean ± SEM. *p<0.05, **p<0.01, ***p<0.001, ****p<0.0001.

Figure S1. The *Ptf1a*^{CreER} allele labeled acinar cells and PanINs in 43.5-week-old mice.

A-B, Representative whole section (top) and high-magnification (bottom) images of immunohistochemical staining for GFP expressed from nTnG lineage tracing allele in 43.5-week-old male (**A**) and female (**B**) PK-*Insr*$^{w/w}$, PK-*Insr*$^{w/f}$, and PK-*Insr*$^{f/f}$ mice. **C-D**, Representative whole section (top) and high-magnification (bottom) images for immunohistochemical staining for GFP expressed from nTnG lineage tracing allele in 43.5-week-old male (**C**) and female (**D**) *Ptf1a*^{CreER};*Insr*$^{w/w}$;nTnG and *Ptf1a*^{CreER};*Insr*$^{f/f}$;nTnG mice. **E-F**, Representative whole section (top) and high-magnification (bottom) H&E images of pancreatic slides from 43.5-week-old male (**E**) and female (**F**) *Ptf1a*^{CreER};*Insr*$^{w/w}$;nTnG and *Ptf1a*^{CreER};*Insr*$^{f/f}$;*nTnG* mice. Scale bars: 2 mm (top) and 0.1mm (bottom).

Figure S2. Loss of *Insr* in acinar cells reduced ductal metaplasia and Alcian blue$^+$ PanIN lesions.

A-B, Representative whole section (top) and high-magnification (bottom) images of immunohistochemical staining of Ck19 for male (**A**) and female (**B**) PK-*Insr*$^{w/w}$, PK-*Insr*$^{w/f}$, and PK-*Insr*$^{f/f}$ mice. **C-D,** Representative whole section (top) and high-magnification (bottom) images of pancreatic slides from male (**C**) and female (**D**) PK-*Insr*$^{w/w}$, PK-*Insr*$^{w/f}$, and PK-*Insr*$^{f/f}$ mice stained with Alcian blue. **E,** Quantification of Ck19$^+$ area for mice from each genotype and sex (M or F) (n= 5-15). **F,** Quantification of Alcian blue$^+$ area for mice from each genotype and sex (M or F) (n= 5-16). **G-H,** The correlation of acinar cell area and Ck19$^+$ area for male (**G**) and female (**H**) mice. The maximum value for Ck19$^+$ area was ~20-30% due to stromal expansion in the parenchyma around the Ck19$^+$ area. Scale bars: 2 mm (top) and 0.1 mm (bottom). Values are shown as mean ± SEM. *p<0.05, **p<0.01, ***p<0.001, ****p<0.0001.

Figure S3. *Insr* loss does not affect pancreatic weight or Cpa1$^+$ area in 12-week-old mice.

A-B, Representative whole section (top) and high-magnification (bottom) images of immunohistochemical staining for GFP expressed from the nTnG lineage tracing allele in 12-week-old male (**A**) and female (**B**) PK-*Insr*$^{w/w}$, PK-*Insr*$^{w/f}$, and PK-*Insr*$^{f/f}$ pancreata. **C-D,** Representative high-magnification images of immunohistochemical staining of Cpa1 for male (**C**) and female (**D**) PK-*Insr*$^{w/w}$, PK-*Insr*$^{w/f}$, and PK-*Insr*$^{f/f}$ mice. **E,** Quantification of Cpa1$^+$ area for mice from each genotype and sex (M or F) (n= 4-7). **F,** The correlation of PanIN area and Cpa1$^+$ area for each genotype and sex (M or F) mice. **G,** The ratio of pancreatic weight to mouse body weight for male (M) and female (F) *Ptf1a*^{CreER};*Insr*$^{w/w}$;nTnG*, Ptf1a*^{CreER};*Insr*$^{f/f}$;nTnG mice, PK-*Insr*$^{w/w}$, PK-*Insr*$^{w/f}$, and PK-*Insr*$^{f/f}$ mice (n= 3-15). Scale bars: 2 mm (top) and 0.1 mm (bottom).

Figure S4. Loss of *Insr* in acinar cells reduced pAkt and pErk.

A-D, Representative whole section (top) and high-magnification (bottom) images of immunohistochemical staining for pAkt (**A-B**) or pErk (**C-D**) in 12-week-old male (**A, C**) and female (**B, D**) PK-*Insr*$^{w/w}$, PK-*Insr*$^{w/f}$, and PK-*Insr*$^{f/f}$ pancreata. **E-F**, Quantification of pAkt$^+$ (**E**) or pErk$^+$ (**F**) pancreatic area for mice from each genotype and sex (M or F) (n= 4-7). Scale bars: 2 mm (top) and 0.1 mm (bottom). **p<0.01.

Figure S5. *Kras*^{G12D} mutant mice had similar proteomics and phospho-proteomics changes as human PDAC tumor samples.

A, Plot of the top 20 mouse pathways from Reactome pathway enrichment for proteins that were significantly up-or down-regulated (Adj. p<0.05) in PK-*Insr*$^{w/w}$ mice (n=3) compared to *Ptf1a*^{CreER};*Insr*$^{w/w}$;nTnG mice (n=3). The FDR for the same pathways from pathway enrichment with

proteins from human data that were significantly up- or down-regulated (Adj. $p<10^{-19}$) in normal (n=75) compared to tumor samples (n=140) are also shown. The size of each dot represents the proportion of genes inputted in all the genes found in each pathway. **B,** Plot of the top 20 mouse pathways from Reactome pathway enrichment for proteins from corresponding phospho-sites that were significantly up- or down-regulated (Adj. p<0.05) in PK-*Insr*$^{w/w}$ mice (n=3) compared to *Ptf1a*^{CreER};*Insr*$^{w/w}$;nTnG mice (n=3). The FDR for the same pathways from pathway enrichment with proteins from corresponding phospho-sites from human data that were significantly up- or down-regulated (Adj. $p<10^{-12}$) in normal (n=75) compared to tumor samples (n=140) are also shown. The size of each dot represents the proportion of genes inputted in all the genes found in each pathway.

Figure S6. Loss of *Insr* in acinar cells reduced desmoplasia and inflammation.

A-B, Representative high-magnification images of immunohistochemical staining of F4/80 (**A-B**) and αSMA (**C-D**) for 12-week-old male (**A, C**) and female (**B, D**) PK-*Insr*$^{w/w}$, PK-*Insr*$^{w/f}$, and PK-*Insr*$^{f/f}$ mice. **E,** Quantification of F4/80^{+} pancreatic area for mice from each genotype and sex (M or F) (n= 4-7). **F,** Quantification of αSMA^{+} pancreatic area for mice from each genotype and sex (M or F) (n= 4-7). *p<0.05, **p<0.01, ***p<0.001.

Figure S7. Female acinar cells are more responsive to TGF-α *ex vivo* than male acinar cells.

A, Quantification of ADM transformation rate of all acinar clusters per well. Acinar clusters were isolated from wild-type Bl6 female (n=4) or male (n=4) mice. Acinar cell 3D explants were quantified after 5 days treatment with a combination of ± TGF-α with soybean trypsin inhibitor in RPMI media.

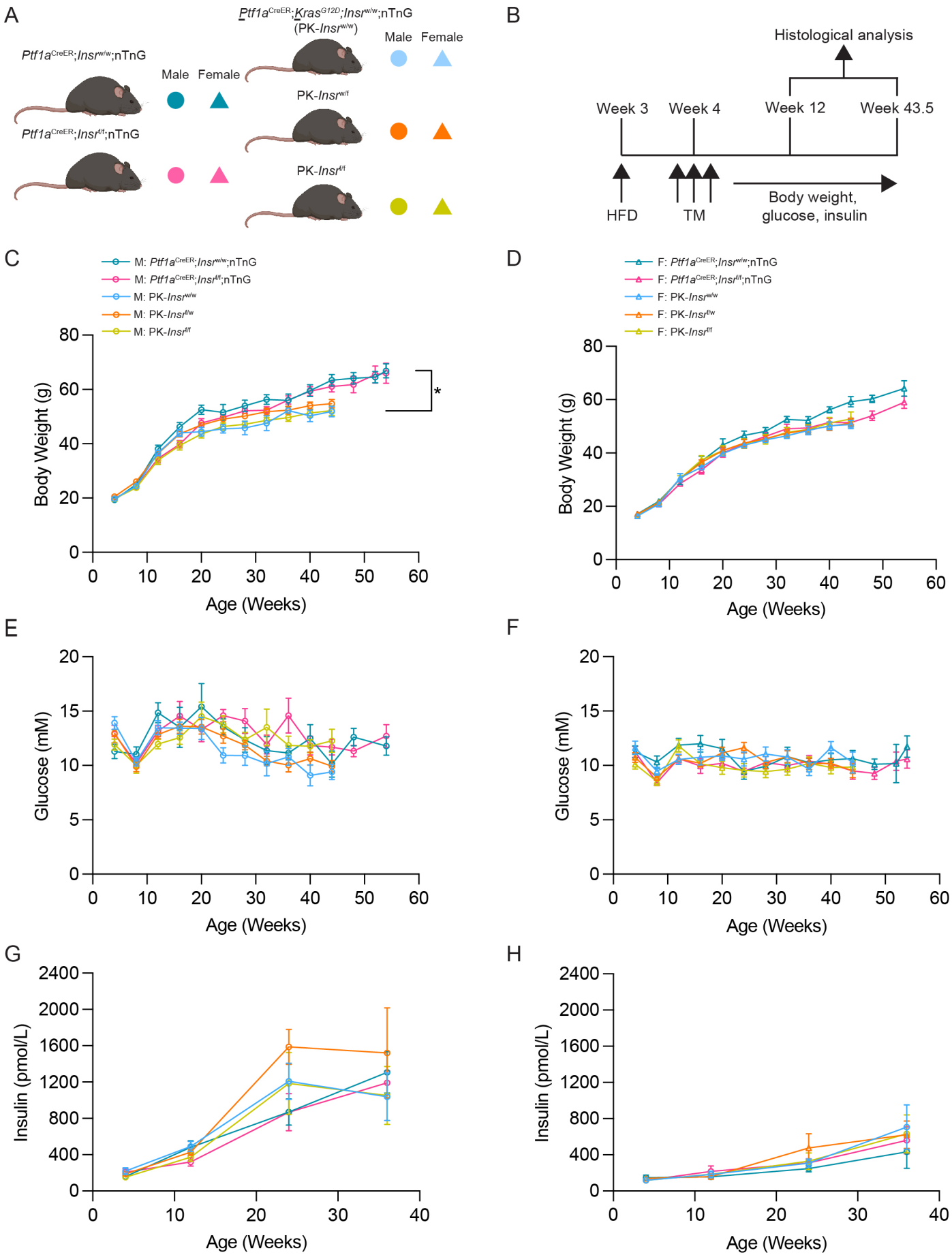
A
Ptf1aCreER;Insrw/w;nTnG
Male Female
Ptf1aCreER;Insrf/f;nTnG
Ptf1aCreER;KrasG12D;Insrw/w;nTnG
(PK-Insrw/w)
Male Female
PK-Insrw/f
PK-Insrf/f
B
Histological analysis
Week 3
Week 4
Week 12
Week 43.5
HFD
TM
Body weight,
glucose, insulin
C
M: Ptf1aCreER;Insrw/w;nTnG
M: Ptf1aCreER;Insrf/f;nTnG
M: PK-Insrw/w
M: PK-Insrf/w
M: PK-Insrf/f
Body Weight (g)
Age (Weeks)
*
D
F: Ptf1aCreER;Insrw/w;nTnG
F: Ptf1aCreER;Insrf/f;nTnG
F: PK-Insrw/w
F: PK-Insrf/w
F: PK-Insrf/f
Body Weight (g)
Age (Weeks)
E
Glucose (mM)
Age (Weeks)
F
Glucose (mM)
Age (Weeks)
G
Insulin (pmol/L)
Age (Weeks)
H
Insulin (pmol/L)
Age (Weeks)

Figure 1

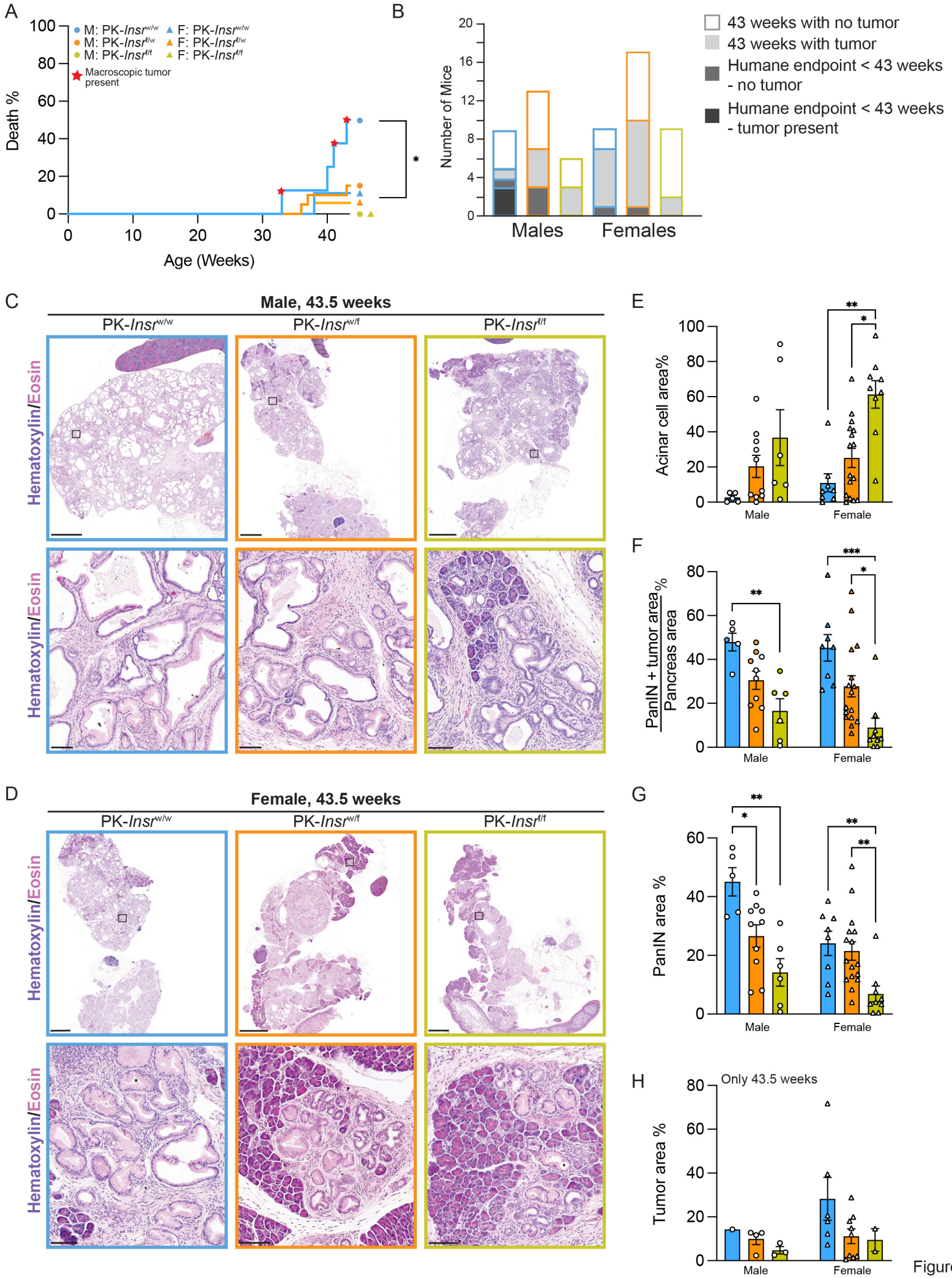
A
M: PK-Insr w/w
M: PK-Insr f/w
M: PK-Insr f/f
F: PK-Insr w/w
F: PK-Insr f/w
F: PK-Insr f/f
Macroscopic tumor present
Death %
Age (Weeks)
*
B
Number of Mice
Males
Females
43 weeks with no tumor
43 weeks with tumor
Humane endpoint < 43 weeks - no tumor
Humane endpoint < 43 weeks - tumor present
C
Male, 43.5 weeks
PK-Insr w/w
PK-Insr w/f
PK-Insr f/f
Hematoxylin/Eosin
D
Female, 43.5 weeks
E
Acinar cell area%
Male
Female
F
PanIN + tumor area / Pancreas area %
G
PanIN area %
H
Only 43.5 weeks
Tumor area %

Figure 2

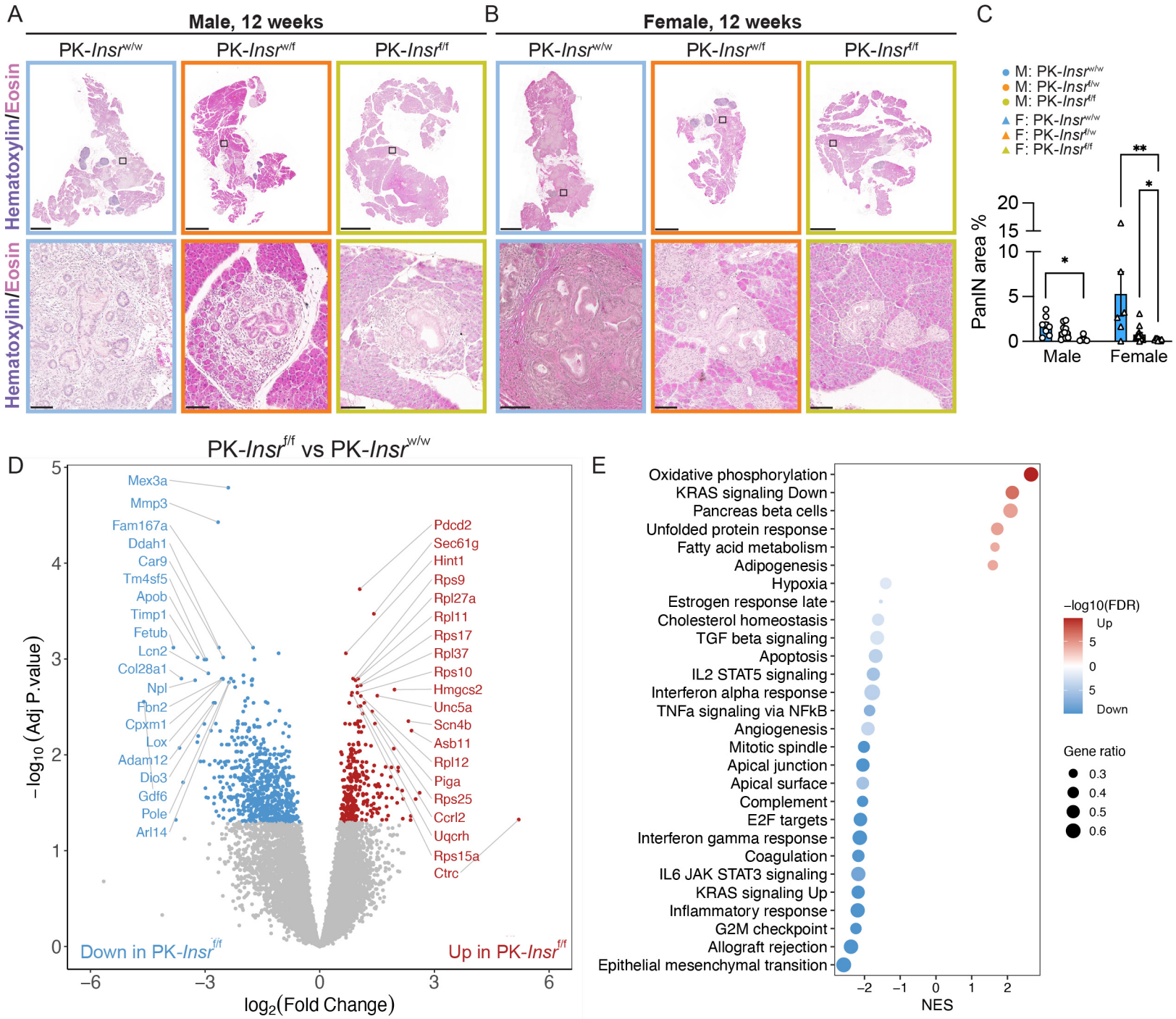
A
Male, 12 weeks
PK-Insr w/w
PK-Insr w/f
PK-Insr f/f
Hematoxylin/Eosin
B
Female, 12 weeks
C
M: PK-Insr w/w
M: PK-Insr f/w
M: PK-Insr f/f
F: PK-Insr w/w
F: PK-Insr f/w
F: PK-Insr f/f
PanIN area %
Male
Female
D
PK-Insr f/f vs PK-Insr w/w
Mex3a
Mmp3
Fam167a
Ddah1
Car9
Tm4sf5
Apob
Timp1
Fetub
Lcn2
Col28a1
Npl
Fbn2
Cpxm1
Lox
Adam12
Dio3
Gdf6
Pole
Arl14
Pdcd2
Sec61g
Hint1
Rps9
Rpl27a
Rpl11
Rps17
Rpl37
Rps10
Hmgcs2
Unc5a
Scn4b
Asb11
Rpl12
Piga
Rps25
Ccrl2
Uqcrh
Rps15a
Ctrc
Down in PK-Insr f/f
Up in PK-Insr f/f
−log10 (Adj P.value)
log2(Fold Change)
E
Oxidative phosphorylation
KRAS signaling Down
Pancreas beta cells
Unfolded protein response
Fatty acid metabolism
Adipogenesis
Hypoxia
Estrogen response late
Cholesterol homeostasis
TGF beta signaling
Apoptosis
IL2 STAT5 signaling
Interferon alpha response
TNFa signaling via NFkB
Angiogenesis
Mitotic spindle
Apical junction
Apical surface
Complement
E2F targets
Interferon gamma response
Coagulation
IL6 JAK STAT3 signaling
KRAS signaling Up
Inflammatory response
G2M checkpoint
Allograft rejection
Epithelial mesenchymal transition
NES
−log10(FDR)
Up
Down
Gene ratio

Figure 3

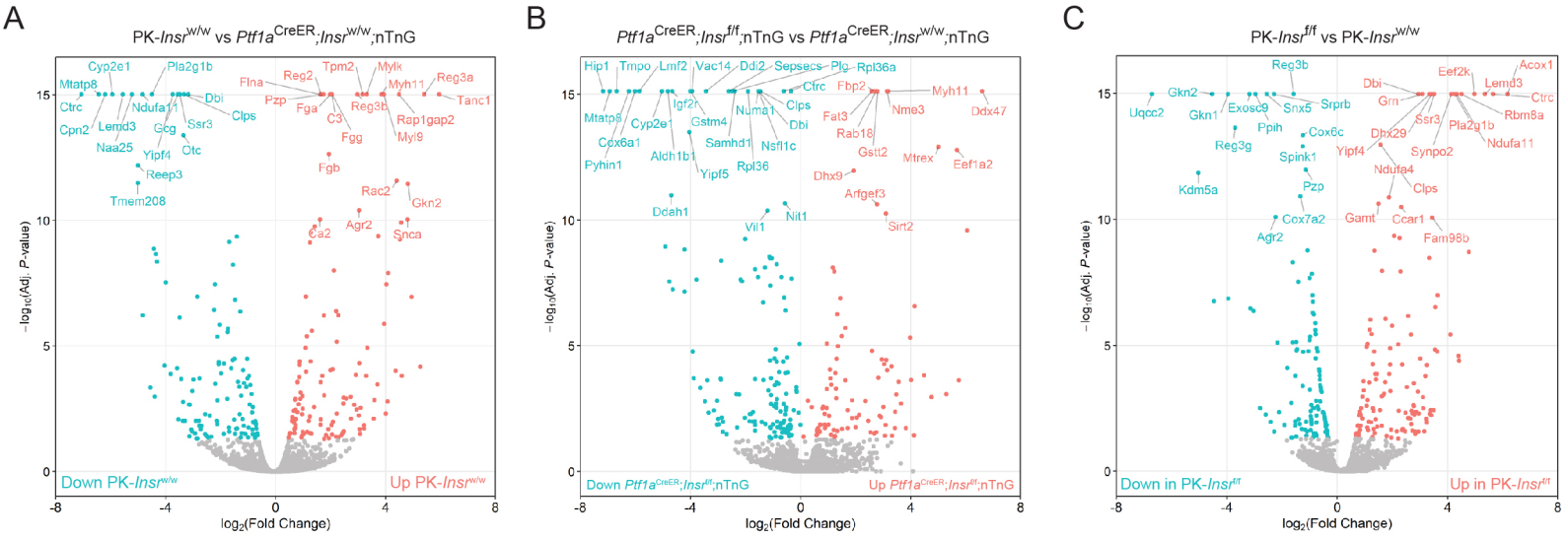
A
PK-Insr w/w vs Ptf1a CreER;Insr w/w;nTnG
Down PK-Insr w/w
Up PK-Insr w/w
B
Ptf1a CreER;Insr f/f;nTnG vs Ptf1a CreER;Insr w/w;nTnG
Down Ptf1a CreER;Insr f/f;nTnG
Up Ptf1a CreER;Insr f/f;nTnG
C
PK-Insr f/f vs PK-Insr w/w
Down in PK-Insr f/f
Up in PK-Insr f/f
log2(Fold Change)
−log10(Adj. P-value)

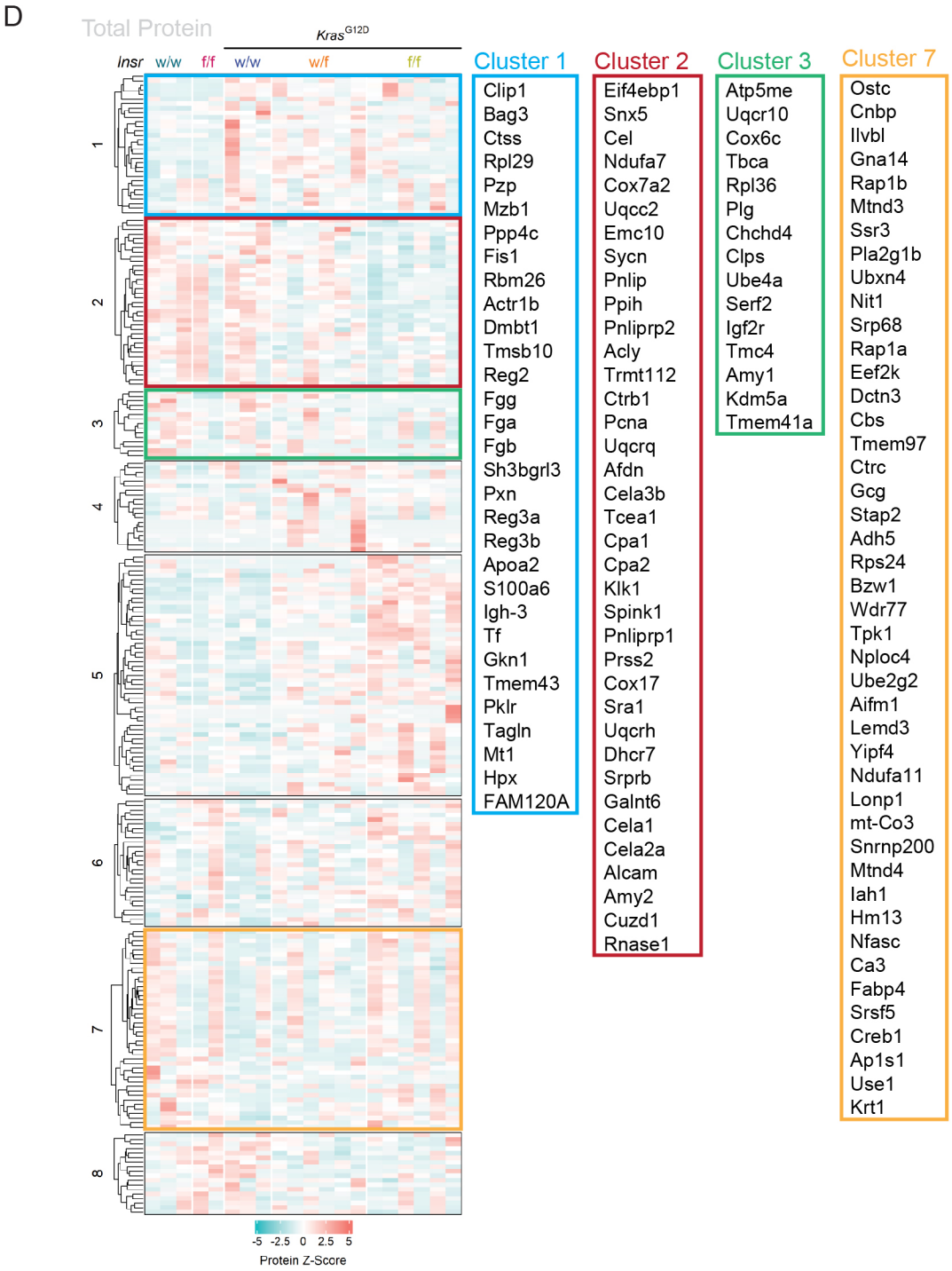
D
Total Protein
Kras G12D
Insr w/w f/f w/w w/f f/f
Cluster 1
Clip1
Bag3
Ctss
Rpl29
Pzp
Mzb1
Ppp4c
Fis1
Rbm26
Actr1b
Dmbt1
Tmsb10
Reg2
Fgg
Fga
Fgb
Sh3bgrl3
Pxn
Reg3a
Reg3b
Apoa2
S100a6
Igh-3
Tf
Gkn1
Tmem43
Pklr
Tagln
Mt1
Hpx
FAM120A
Cluster 2
Eif4ebp1
Snx5
Cel
Ndufa7
Cox7a2
Uqcc2
Emc10
Sycn
Pnlip
Ppih
Pnliprp2
Acly
Trmt112
Ctrb1
Pcna
Uqcrq
Afdn
Cela3b
Tcea1
Cpa1
Cpa2
Klk1
Spink1
Pnliprp1
Prss2
Cox17
Sra1
Uqcrh
Dhcr7
Srprb
Galnt6
Cela1
Cela2a
Alcam
Amy2
Cuzd1
Rnase1
Cluster 3
Atp5me
Uqcr10
Cox6c
Tbca
Rpl36
Plg
Chchd4
Clps
Ube4a
Serf2
Igf2r
Tmc4
Amy1
Kdm5a
Tmem41a
Cluster 7
Ostc
Cnbp
Ilvbl
Gna14
Rap1b
Mtnd3
Ssr3
Pla2g1b
Ubxn4
Nit1
Srp68
Rap1a
Eef2k
Dctn3
Cbs
Tmem97
Ctrc
Gcg
Stap2
Adh5
Rps24
Bzw1
Wdr77
Tpk1
Nploc4
Ube2g2
Aifm1
Lemd3
Yipf4
Ndufa11
Lonp1
mt-Co3
Snrnp200
Mtnd4
Iah1
Hm13
Nfasc
Ca3
Fabp4
Srsf5
Creb1
Ap1s1
Use1
Krt1
-5 -2.5 0 2.5 5
Protein Z-Score

Figure 4

A

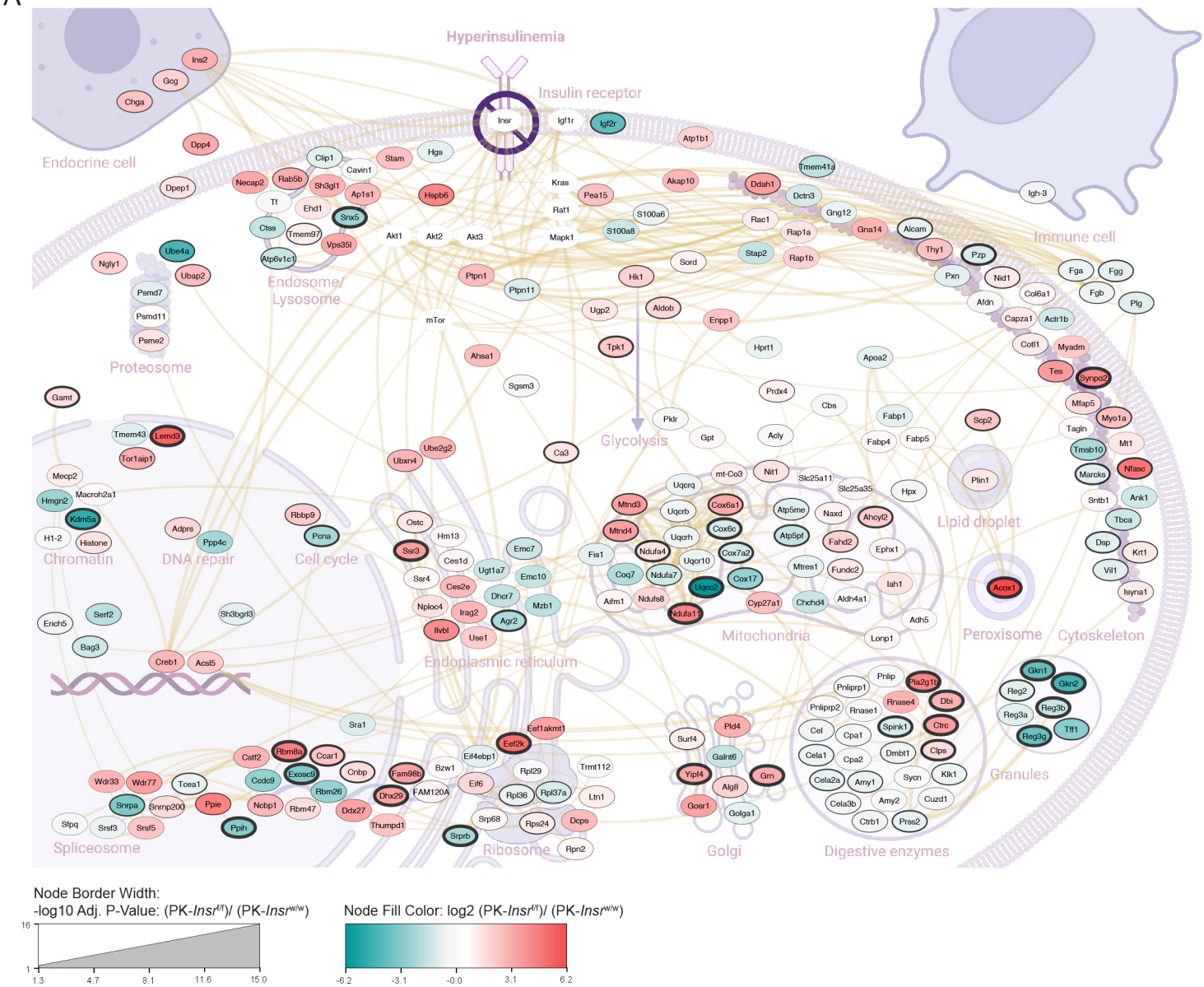
Hyperinsulinemia
Insulin receptor
Endocrine cell
Immune cell
Endosome/
Lysosome
Proteosome
Glycolysis
Chromatin
DNA repair
Cell cycle
Lipid droplet
Mitochondria
Peroxisome
Cytoskeleton
Endoplasmic reticulum
Granules
Spliceosome
Ribosome
Golgi
Digestive enzymes
Node Border Width:
-log10 Adj. P-Value: (PK-Insr f/f)/ (PK-Insr w/w)
16
1
1.3
4.7
8.1
11.6
15.0
Node Fill Color: log2 (PK-Insr f/f)/ (PK-Insr w/w)
-6.2
-3.1
-0.0
3.1
6.2

B

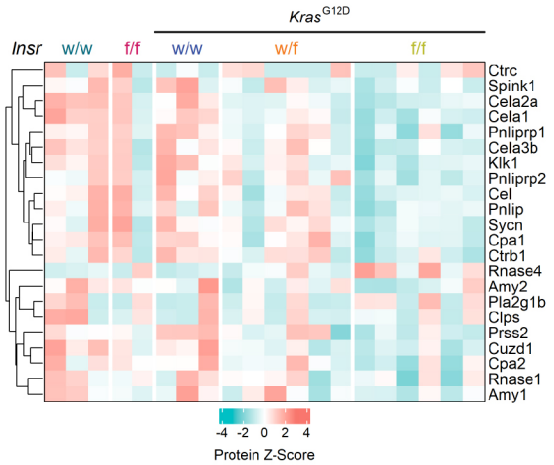
Kras G12D
Insr
w/w
f/f
w/w
w/f
f/f
Ctrc
Spink1
Cela2a
Cela1
Pnliprp1
Cela3b
Klk1
Pnliprp2
Cel
Pnlip
Sycn
Cpa1
Ctrb1
Rnase4
Amy2
Pla2g1b
Clps
Prss2
Cuzd1
Cpa2
Rnase1
Amy1
-4 -2 0 2 4
Protein Z-Score

C

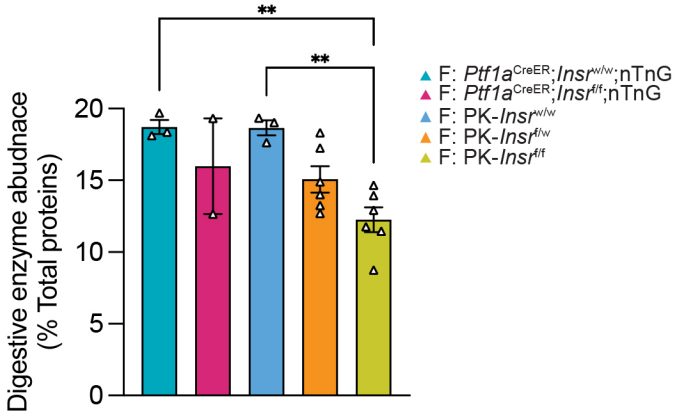
**
**
Digestive enzyme abudnace
(% Total proteins)
20
15
10
5
0
F: Ptf1a CreER;Insr w/w;nTnG
F: Ptf1a CreER;Insr f/f;nTnG
F: PK-Insr w/w
F: PK-Insr f/w
F: PK-Insr f/f

Figure 5

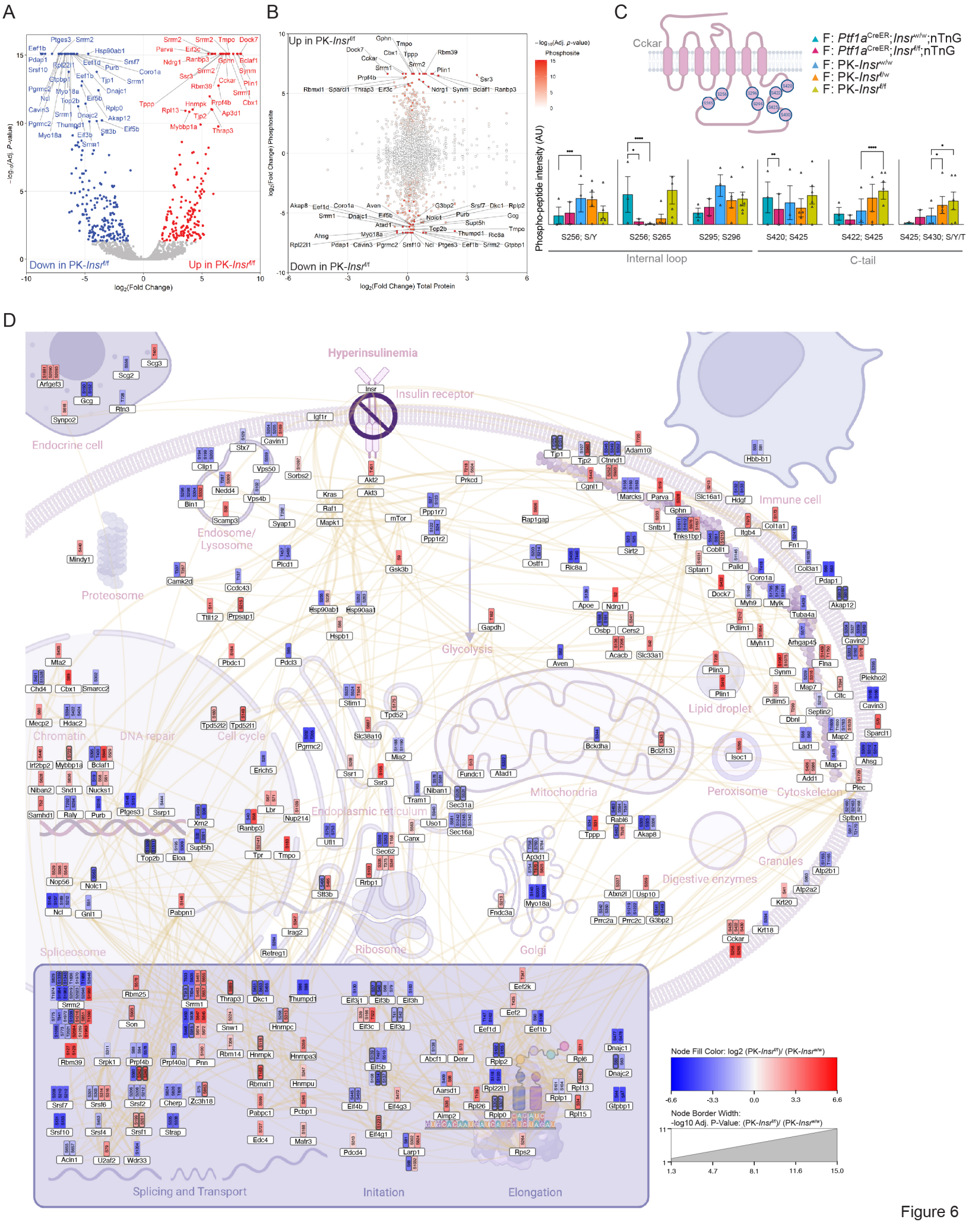
A
Down in PK-Insr f/f
Up in PK-Insr f/f
log2(Fold Change)
−log10(Adj. P-value)
B
Up in PK-Insr f/f
Down in PK-Insr f/f
log2(Fold Change) Phosphosite
log2(Fold Change) Total Protein
−log10(Adj. p-value)
Phosphosite
C
Cckar
F: Ptf1aCreER;Insrw/w;nTnG
F: Ptf1aCreER;Insrf/f;nTnG
F: PK-Insrw/w
F: PK-Insrf/w
F: PK-Insrf/f
Phospho-peptide intensity (AU)
S256; S/Y
S256; S265
S295; S296
S420; S425
S422; S425
S425; S430; S/Y/T
Internal loop
C-tail
D
Hyperinsulinemia
Insulin receptor
Endocrine cell
Endosome/ Lysosome
Proteosome
Immune cell
Glycolysis
Lipid droplet
Chromatin
DNA repair
Cell cycle
Mitochondria
Peroxisome
Cytoskeleton
Endoplasmic reticulum
Granules
Digestive enzymes
Spliceosome
Ribosome
Golgi
Splicing and Transport
Initation
Elongation
Node Fill Color: log2 (PK-Insrf/f)/ (PK-Insrw/w)
-6.6
-3.3
0.0
3.3
6.6
Node Border Width:
-log10 Adj. P-Value: (PK-Insrf/f)/ (PK-Insrw/w)
1.3
4.7
8.1
11.6
15.0

Figure 6

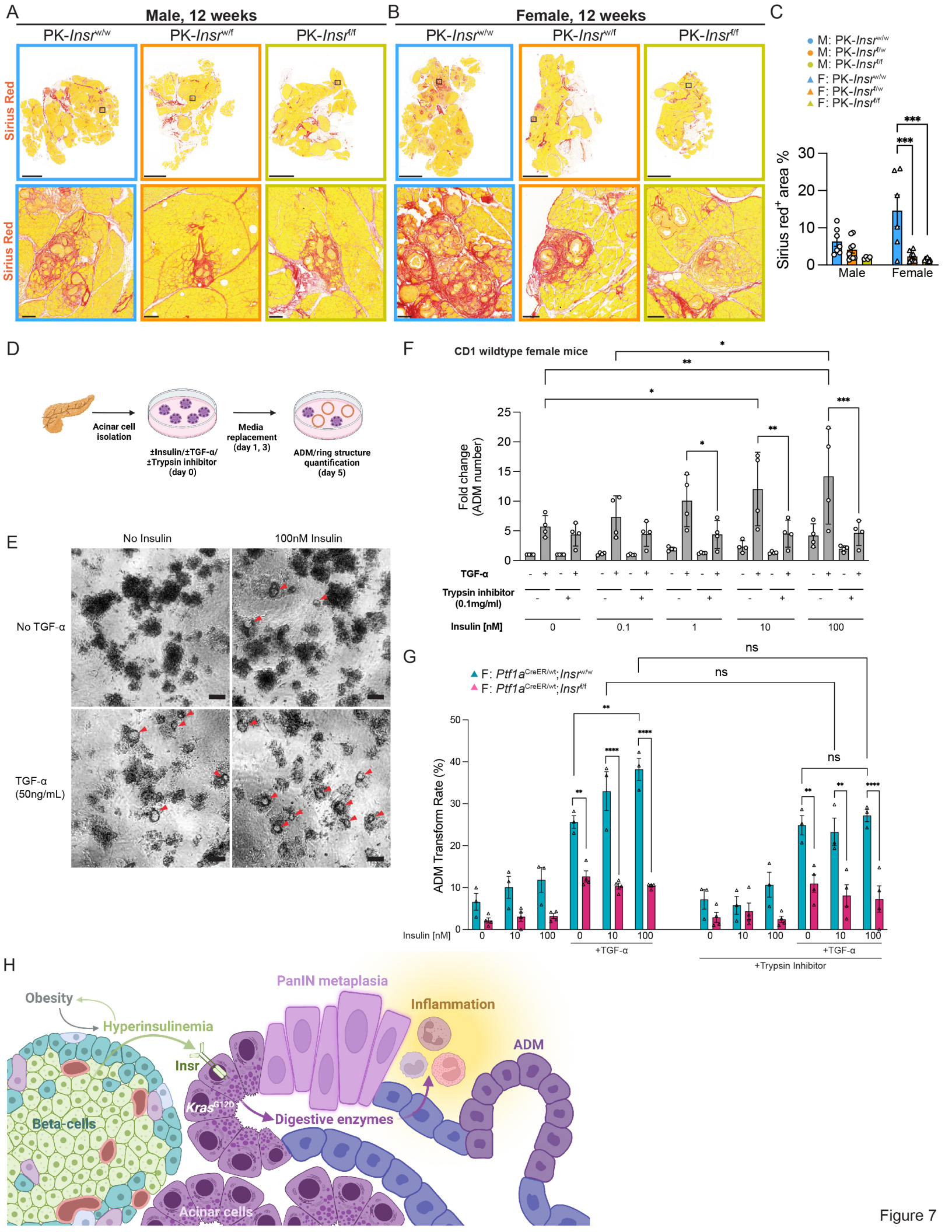
A
Male, 12 weeks
PK-Insr w/w
PK-Insr w/f
PK-Insr f/f
Sirius Red
Sirius Red
B
Female, 12 weeks
PK-Insr w/w
PK-Insr w/f
PK-Insr f/f
C
M: PK-Insr w/w
M: PK-Insr f/w
M: PK-Insr f/f
F: PK-Insr w/w
F: PK-Insr f/w
F: PK-Insr f/f
Sirius red+ area %
Male
Female
D
Acinar cell isolation
±Insulin/±TGF-α/ ±Trypsin inhibitor (day 0)
Media replacement (day 1, 3)
ADM/ring structure quantification (day 5)
E
No Insulin
100nM Insulin
No TGF-α
TGF-α (50ng/mL)
F
CD1 wildtype female mice
Fold change (ADM number)
TGF-α
Trypsin inhibitor (0.1mg/ml)
Insulin [nM]
G
F: Ptf1a CreER/wt;Insr w/w
F: Ptf1a CreER/wt;Insr f/f
ADM Transform Rate (%)
Insulin [nM]
+TGF-α
+Trypsin Inhibitor
ns
H
Obesity
Hyperinsulinemia
Insr
Beta-cells
PanIN metaplasia
Inflammation
ADM
Kras G12D
Digestive enzymes
Acinar cells

Figure 7